Stellenbosch
UNIVERSITY
IYUNIVESITHI
UNIVERSITEIT

Pilot Study for Ship Fatigue Life Analysis through Acceleration Measurements

Mechanical Project 478

Final Report Progress

Author:
Mr H.C. Janse van Vuuren
21642478

Supervisor:
Prof A. Bekker

21 October 2022

saam vorentoe · masiye phambili · forward together

Department of Mechanical and Mechatronic Engineering
Departement Meganiese en Megatroniese Ingenieurswese
Privaatsak X1, Private Bag X1, Matieland, 7602
Tel: +27 21 808 4204 | www.eng.sun.ac.za

Plagiarism declaration

I have read and understand the Stellenbosch University Policy on Plagiarism and the definitions of plagiarism and self-plagiarism contained in the Policy [Plagiarism: The use of the ideas or material of others without acknowledgement, or the re-use of one's own previously evaluated or published material without acknowledgement or indication thereof (self-plagiarism or text-recycling).

I also understand that direct translations are plagiarism, unless accompanied by an appropriate acknowledgement of the source. I also know that verbatim copy that has not been explicitly indicated as such, is plagiarism.

I know that plagiarism is a punishable offence and may be referred to the University's Central Disciplinary Committee (CDC) who has the authority to expel me for such an offence.

I know that plagiarism is harmful for the academic environment and that it has a negative impact on any profession.

Accordingly, all quotations and contributions from any source whatsoever (including the internet) have been cited fully (acknowledged); further, all verbatim copies have been expressly indicated as such (e.g. through quotation marks) and the sources are cited fully.

I declare that, except where a source has been cited, the work contained in this assignment is my own work and that I have not previously (in its entirety or in part) submitted it for grading in this module/assignment or another module/assignment.

I declare that have not allowed, and will not allow, anyone to use my work (in paper, graphics, electronic, verbal or any other format) with the intention of passing it off as his/her own work.

I know that a mark of zero may be awarded to assignments with plagiarism and also that no opportunity be given to submit an improved assignment.

Signature: 

Name: HC Janse van Vuuren

Student no: 21642478

Date: 27/09/2022

Executive summary

Title of project
Pilot study of ship fatigue life analysis through acceleration measurements on a beam.
Objectives
This project had the overarching goal of investigating an alternative method for obtaining accumulated fatigue damage of an easily modelled structure from accelerometer measurements instead of traditional strain gauge measurements for structures in operation experiencing cyclic loads. To achieve that goal, an intermediate objective was required for obtaining the location of maximum strain in the structure to be monitored for damage. The location for maximum strain was fist determined analytically and then verified experimentally.
What is current practice and what are its limitations?
In current practice, experimental strain mode shapes are determined from strain measurement time histories and not from acceleration measurements.
What aspects of your project are new/unique?
This project attempted to transform experimentally determined displacement mode shapes of a simple structure to find a transformed strain mode shape.
Was the project successful? How will it make a difference?
The project was a partial success. An alternative experimental method was formulated for determining the strain mode shape of a beam, allowing for better insights gained from existing historical acceleration measurements. An alternative method for determining accumulated fatigue damage from accelerometer measurements was evaluated and compared to a traditional strain gauge sensor network and found to be unreliable. It is therefore recommended to make use of traditional strain gauge networks for operational fatigue monitoring.
What were the risks to the project being a success? How were these handled?
Breakdown of computer and test equipment was one of the biggest risks that could have prevented the successful completion of this project. This was mitigated by carefully planning experiments, applying the hierarchy of control to identified risks and adhering to laboratory rules and practices.
Which aspects of the project will carry on after completion and why?
This project will inform decisions made in the design of a hull monitoring system for operational fatigue damage estimation on the SA Agulhas II polar supply and research vessel.
What arrangements have been/will be made to expedite continuation?
The findings of this investigation is documented and communicated in this final report and presentation. Experimental data is backed up electronically, uploaded on GitHub and included in the project submission files. The experimental rig will remain in the laboratory for future use.

ECSA exit level outcomes

ECSA outcomes assessed in this module:	
ECSA outcome:	**Addressed in chapter:**
ELO 1. Problem solving: Demonstrate competence to identify, assess, formulate and solve convergent and divergent engineering problems creatively and innovatively.	1, 3, 4 Problem statement and steps taken to address/solve problem.
ELO 2. Application of scientific and engineering knowledge: Demonstrate competence to apply knowledge of mathematics, basic science and engineering sciences from first principles to solve engineering problems.	3, 4, Appendix A
ELO 3. Engineering design: Demonstrate competence to perform creative, procedural and non-procedural design and synthesis of components, systems, engineering works, products or processes.	Algorithms developed in chapter 3. Experiment design in chapter 4.
ELO 5. Engineering methods, skills and tools, including information technology: Demonstrate competence to use appropriate engineering methods, skills and tools, including those based on information technology.	3, 4 Siemens Testlab – Modal analysis and sensor measurements. MATLAB – Calculations and data analysis. Appendix A, B, C, D, E, F
ELO 6. Professional and technical communication: Demonstrate competence to communicate effectively, both orally and in writing, with engineering audiences and the community at large.	Project proposal, progress report, progress presentation, final report draft, final report, final presentation, poster.
ELO 8. Individual, team and multidisciplinary working: Demonstrate competence to work effectively as an individual, in teams and in multi-disciplinary environments.	The author will work individually throughout this project.
ELO 9. Independent learning ability: Demonstrate competence to engage in independent learning through well-developed learning skills.	2, 3, 4, Appendix A

Dedication

Dedicated to God, may His glory be revealed through the study of creation.

Acknowledgements

The author would like to thank the following individuals:

His parents, Rev L.J. Janse van Vuuren and Mrs D.M. Janse van Vuuren for their support and financing of his studies and in effect a portion of this project.

Prof A. Bekker for her support, guidance and feedback throughout the project.

Dr B. Nickerson for his advice and insightful discussions regarding the project.

The sound and vibration laboratory engineer, Mr J. Laas, for his time and advice during the laboratory experiments.

Table of contents

Page

List of figures

Page

List of tables

Page

Nomenclature

Abbreviation

DAS	Data Acquisition System
DMS	Displacement Mode Shape
EMA	Experimental Modal Analysis
EMF	Electro-Magnetic Field
FFT	Fast Fourier Transform
FRF	Frequency Response Function
GF	Gauge Factor
ICP®	Integrated Circuit-Piezoelectric
MAC	Modal Assurance Criterion
M&M	Mechanical and Mechatronic
PCB	PicoCoulomB (PCB Piezotronics sensor manufacturer)
s.a.	sine anno (no year)
SCADAS	Signal Conditioning and Data Acquisition System
SMS	Strain Mode Shape

Superscripts

T	Transpose

Subscripts

a	Axial
b	Bending
f	Fatigue
n	Natural
O	Origin
T	Thermal
0	Initial / at start of time series

Roman Letters

A	Area
a	SN curve scaling constant
B	SN curve exponent constant
d	Change
E	Youngs' modulus / modulus of elasticity
f	Frequency
I	Moment of inertia
L	Length
M	Moment
m	Mass
N	Cycles
S	Stress
t	Time
V	Voltage
w	Displacement
x	Position along the x axis
y	Position along the y axis
$\dot{y}$	Velocity, the first derivative of position in time
$\ddot{y}$	Acceleration, the second derivative of position in time
z	Position along the z axis

Greek Letters

β	Solution to a transcendental equation
ε	Strain
θ	Angle / slope
ρ	Density
σ	Stress
υ	Poisson's ratio
ω	Angular frequency

1 Introduction

1.1 Background

The use of marine vessels has become an integral part of the world, enabling the connection of economies through activities such as fishing, transport of cargo and passengers as well as research and recreation. The functional scale and operating environment of marine vessel structures are harsh and dynamic and to ensure the safety, longevity and economy of their use require studies such as this one, which includes the consideration of various load cases. Environmental loads are the dominating load category and of these, waves and currents are considered the most important load source for marine structures (Bai & Jin, 2016:509).

Considering the dynamic and cyclic nature of wave loads, fatigue failure modes need to be accounted for in the design and lifetime calculation of a ship through fatigue analysis. In materials, fatigue is the accumulation of damage due to cyclic loading and involves crack initiation, propagation and final fracture failure (Bai & Jin, 2016:477). Due to the shifting support of waves along the length of a ship the global structure experiences bending modes as it hogs and sags with the shifting support as is shown in Figure 1. For this reason, it is reasonable to compare a ship to a beam with free-free boundary conditions.

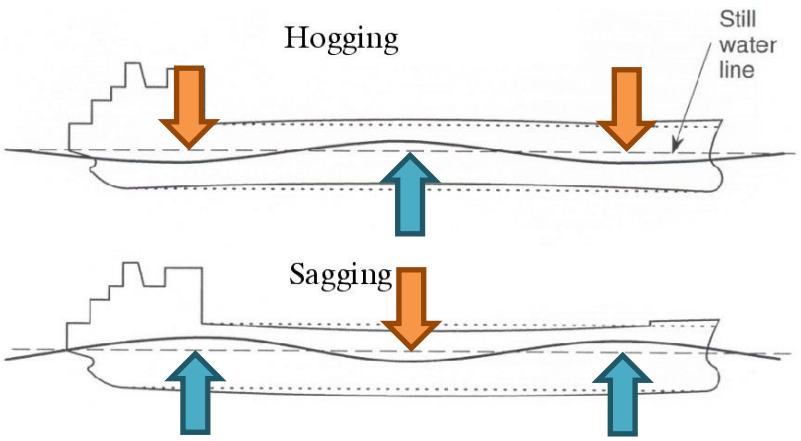

Figure 1: Ship hogging and sagging (Source: Li, 2011)

This project prototypes the testing, data collection and analysis techniques needed to inform decisions made in the design of a hull monitoring system for operational fatigue damage monitoring and estimation on the SA Agulhas II polar supply and research vessel. To achieve this, the correlation between fatigue life estimates and modal properties obtained from accelerometer measurements in

comparison with those obtained from strain measurements of a simple structure, will be investigated. Focus will be afforded to the behaviour of the vertical bending modes of a ship's global structure. For this reason, a simple proxy for the hull structure and its dynamic behaviour will be developed on a beam. This project forms part of the Mechanical Project 478 module of the Department of Mechanical and Mechatronic (M&M) Engineering at the University of Stellenbosch. It is conducted by Mr H.C. Janse van Vuuren, and proposed and supervised by Prof A. Bekker. This project is independent of research done by other students.

1.2 Objectives

The aim of this project is to study an easily modelled structure that is relatable to ships, namely a beam, and evaluate an alternative method for obtaining an estimate of its remaining useful life, or the remaining operational hours to failure. The method will be evaluated through benchmark analysis from analytical models and through the comparison of results from traditional strain gauge networks to accelerometer networks.

To evaluate remaining useful life, one requires information of the stresses experienced by the structure. Since the structure is dynamic and cyclically excited, the bending modes can be considered to determine the location of maximum stress in a beam. By performing a strain modal analysis, the strain mode shapes (SMS) can be obtained and used to inform the placement of strain gauges to obtain the stress measurements needed to evaluate the remaining useful life of the structure, by estimating the fatigue life and fatigue damage number.

In this project, the feasibility of the use of acceleration measurements to obtain the same results of strain gauges in the modal analysis and fatigue life analysis sections of this project will be investigated. Demonstration and evaluation processes will be used to develop an algorithm for data processing in order to determine fatigue damage. Tests to failure are considered to be outside of the scope of this project and the SN curves found in literature are assumed to be accurate for fatigue life estimates of known materials. To achieve this the following objectives have been set:

1. To investigate a method for transforming displacement mode shapes to strain mode shapes.

2. To verify the mode shape transformation method by determining the correlation between strain mode shapes determined from experimental acceleration measurements to those determined from experimental strain measurements.

3. To investigate a method for determining fatigue life estimates and fatigue damage, for a simple structure experiencing cyclic loading from acceleration measurements.

4. To verify the fatigue life estimating method experimentally by determining the correlation between fatigue life estimates and fatigue damage determined from acceleration measurements to those determined from strain measurements.

1.3 Motivation

If successful, this project will inform decisions made in the design of a hull monitoring system for operational fatigue damage estimation and inform the use of acceleration measurements in methods where strain measurements are typically needed. A specific example is the SA Agulhas II, where an accelerometer network is installed in the hull to allow for better insights gained from existing historical acceleration measurements of this vessel and others. During this project, useful skills for conducting future experiments and data analysis will be developed.

2 Literature review

2.1 Ship operational environment

"*Marine structures are exposed to a variety of loads during their life cycles. The loads are commonly classified as:*

- *Functional*
    - *Dead loads*
    - *Live loads*
- *Environmental*
    - *Sea loads (waves and currents)*
    - *Wind loads*
    - *Seismic loads*
- *Accidental*

Major factors that should be considered in marine structural design include:

- *Still water and wave loads, and their possible combinations*
- *Ultimate strength of structural components and systems*
- *Fatigue/fracture in critical structural details.*

For ship structures, the key fatigue loads are global wave loads, local pressure, and internal loads" (Bai & Jin, 2016).

2.2 Euler-Bernoulli beam theory

A long slender element where $L/h_z \geq 10$ and $L/h_y \geq 10$ as is shown in Figure 2 can be modelled as a Euler-Bernoulli beam (Inman, 2014), from here on referred to as a beam.

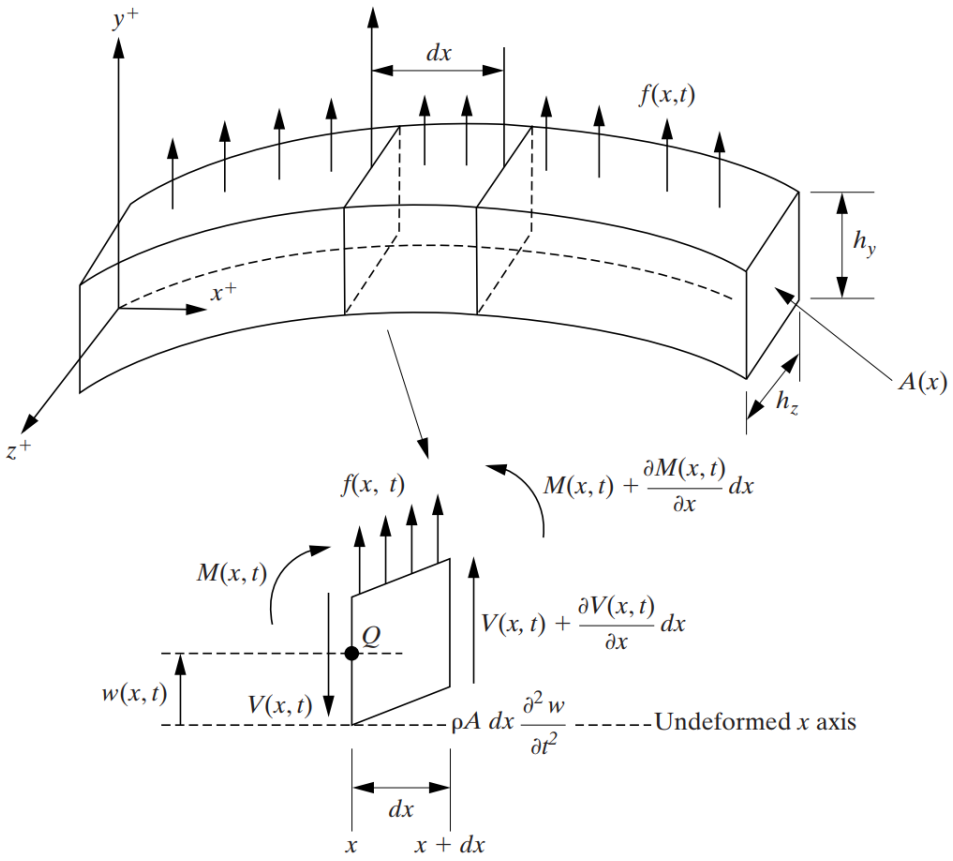

Figure 2: Simple Euler-Bernoulli beam (Source: Inman, 2014:545)

For beams, the load case, shear loading, slope and displacement can be related to each other according to Equations (1) to (5) (Budynas & Nisbett, 2015:164).

$$\frac{d^4y}{dx^4} = \frac{q(x)}{EI} \quad \textbf{(1)}$$

$$\frac{d^3y}{dx^3} = \frac{V(x)}{EI} \quad \textbf{(2)}$$

$$\frac{d^2y}{dx^2} = \frac{M(x)}{EI} \quad \textbf{(3)}$$

$$\frac{dy}{dx} = \theta(x) \quad \textbf{(4)}$$

$$y = f(x) \quad \textbf{(5)}$$

These relations are illustrated in Figure 3.

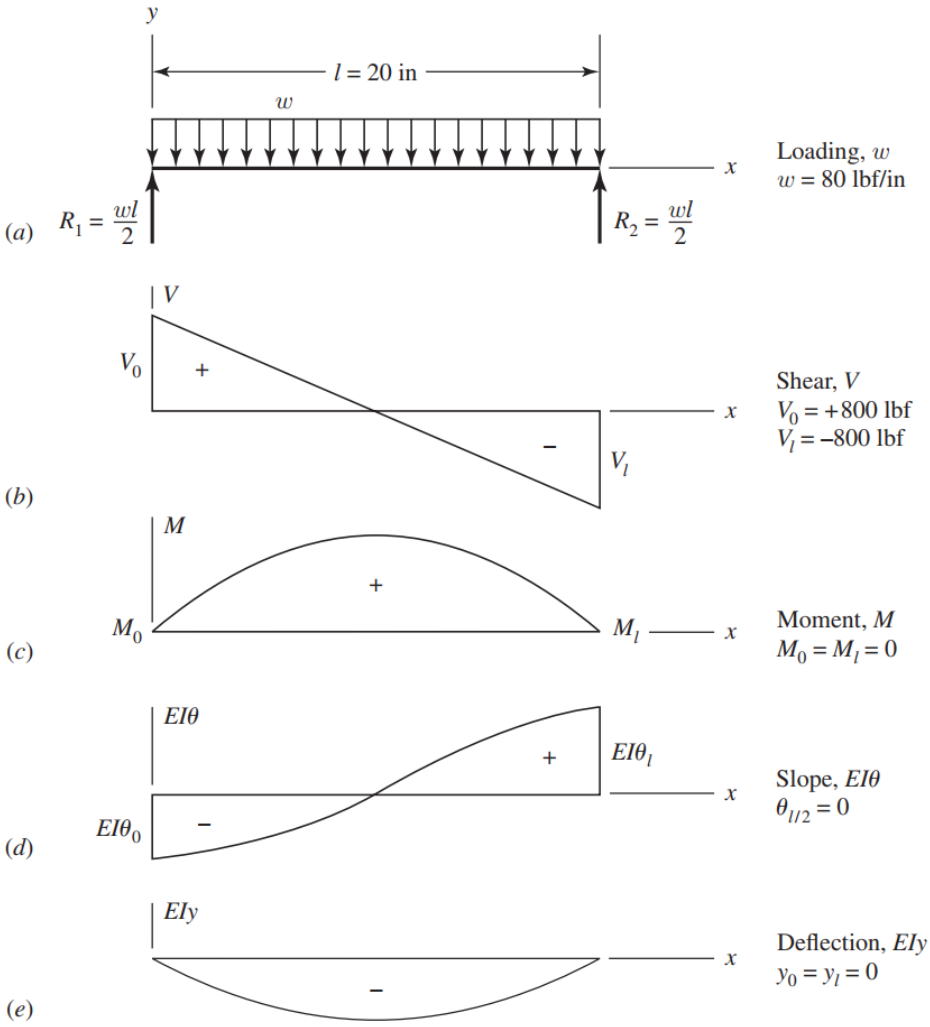

Figure 3: Beam condition relations (Source: Budynas & Nisbett, 2015:165)

Stress, strain, Young's modules and Poisson's ratio:

$$\sigma = \frac{F}{A} \quad (6)$$

$$\sigma = \varepsilon E \quad (7)$$

$$\varepsilon_x = \frac{dx}{x} \quad (8)$$

$$\upsilon = -\frac{\varepsilon_y}{\varepsilon_x} = -\frac{\varepsilon_z}{\varepsilon_x} \quad (9)$$

Bending stress and strain (Budynas & Nisbett, 2015:104):

$$\sigma = -\frac{Mc}{I} = -\frac{d^2y}{dx^2} \cdot cE \qquad (10)$$

$$\varepsilon = -\frac{Mc}{EI} = -\frac{d^2y}{dx^2} \times c \qquad (11)$$

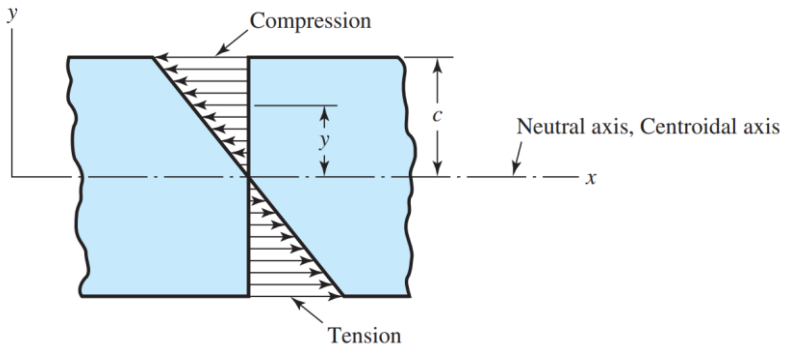

Figure 4: Bending stress in a beam (Source: Budynas & Nisbett, 2015:104)

Since the surface bending stress can so easily be related to strain, strain gauges can be used to determine surface bending stress.

2.3 Metal fatigue

2.3.1 Cyclic loading

Cyclic loading involves periodic stress cycles as is shown in Figure 5.

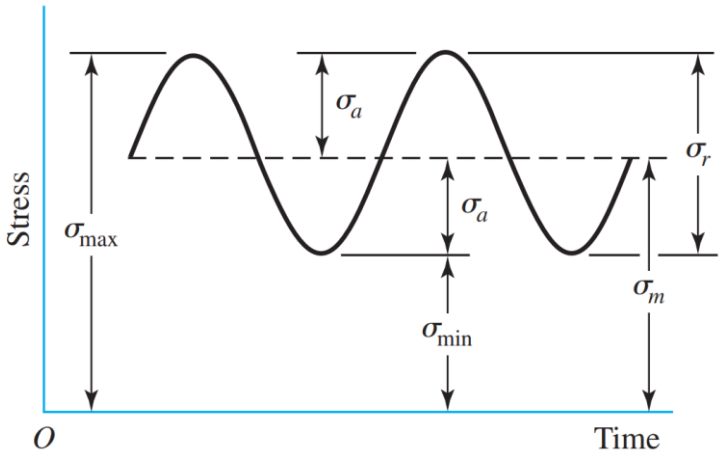

Figure 5: Stress cycles definition (Source: Budynas & Nisbett, 2015)

σ_{min} = minimum stress σ_m = midrange component

σ_{max} = maximum stress σ_r = range of stress

σ_a = amplitude component σ_s = static or steady stress

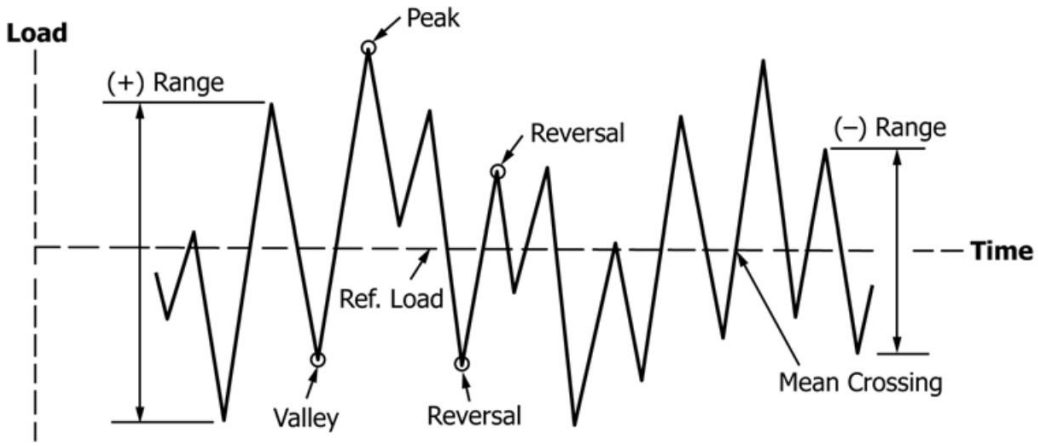

Figure 6: Basic fatigue loading parameters (Source: ASTM, 2011)

-

2.3.2 Wöhler (SN) curve

Design fatigue strength curves (S-N or stress-life curves) can be specified using the standardized parameters from Eurocode 3 EN 1993-1-9, *Design of steel structures – Part 1-9: Fatigue*.

A Wöhler SN curve can be characterised by Equation (12) (Dowling, Kampe, Kral, 2019).

$$S_f = a \cdot N^B \qquad \textbf{(12)}$$

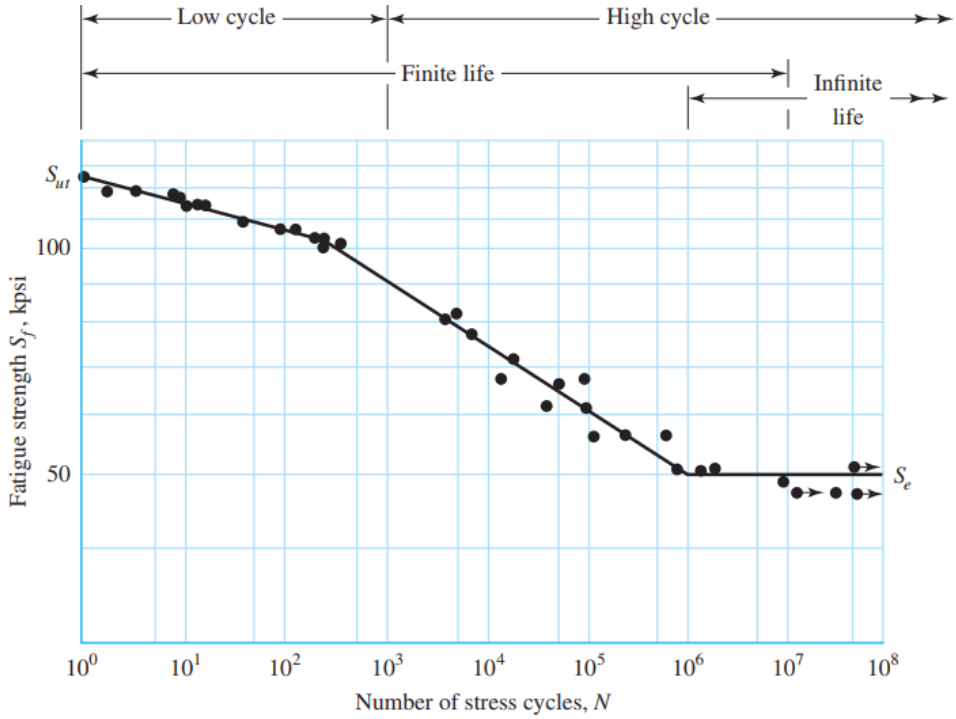

Figure 7: S-N curve example (Source: Budynas & Nisbett, 2015)

2.3.3 Palmgren-Miner's method

Palmgren-Miner's method for linear damage accumulation can be seen in Equations (13) and (14) (Budynas & Nisbett, 2015 and Bai & Jin, 2016).

$$\sum_{i=1}^{k} \frac{n_i}{N_i} = 1 \qquad \textbf{(13)}$$

$$D = \sum_{i=1}^{n} \frac{1}{N(S_i)} \quad (14)$$

2.3.4 Rainflow counting

Cycle counts can be done using a MATLAB rainflow counting algorithm based on ASTM E1049-85, '*Standard Practices for Cycle Counting in Fatigue Analysis*' (MathWorks, [s.a.]).

2.4 Structural vibration

The modal properties of a structure include its natural frequency, damping ratio and mode shapes. The natural frequency is the frequency at which a structure naturally vibrates when excited (impacted or set into motion) and it depends on the mass and stiffness of the structure (Avitabile, 2017). The damping ratio is a dimensionless parameter, characterising how vibration attenuates (dies out) after being excited (Avitabile, 2017). A mode shape is a vector that describes the relative motion between degrees of freedom (Inman, 2014), or more simply put: a mode shape is the deformation pattern of a structure when vibrating at a specific frequency (Avitabile, 2017). Mode shapes are usually a fraction of a sinusoidal wave, as is shown in Figure 8.

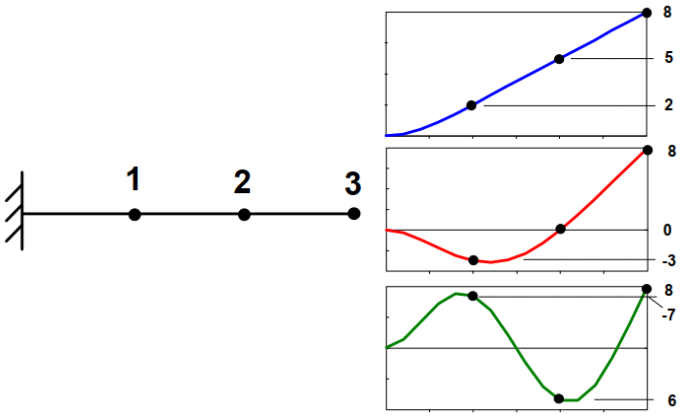

Figure 8: Mode shape example (Source: Avitabile, 2018)

2.4.1 Acceleration modal analysis

Modal analysis is the process of modelling the dynamic response of a structure in terms of its modal parameters (Sorber, [s.a.]) or also referred to as dynamic properties. To calculate the modal properties, one needs to determine the frequency response function (FRF), which is, simply put, the transfer function of

the input frequency to the amplitude of the response out. One can derive different FRFs from a modal analysis, depending on where you hit the test structure and measure the response, as is shown in Figure 9. One only needs one row or column of the matrix to determine all the modal properties (Avitabile, 2017). The general form for the expression of any FRF can be seen in Equation (15) (Ewins, 2000).

$$H_{jk}(\omega) = \frac{X_j}{F_k} = \sum_{r=1}^{N} \frac{{}_rA_{jk}}{\lambda_r^2 - \omega^2} \qquad (15)$$

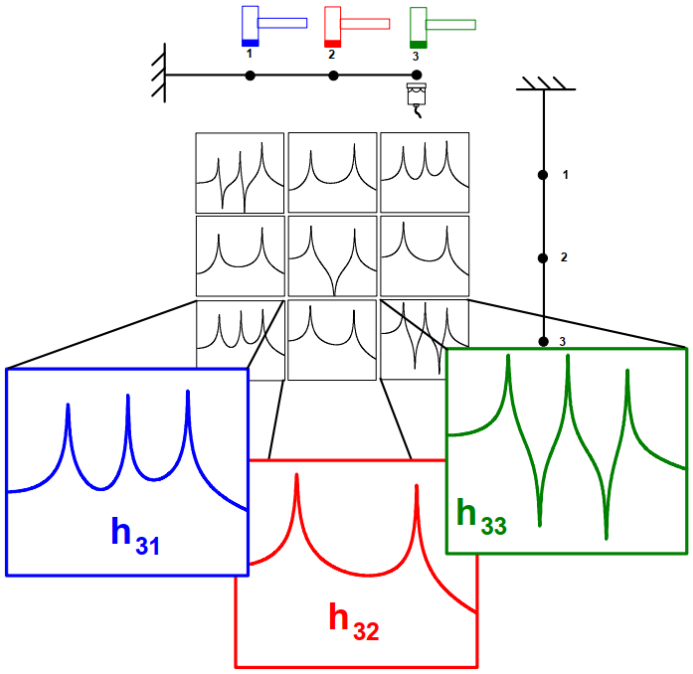

Figure 9: Frequency response function matrix (Source: Avitabile, 2018)

2.4.2 Strain modal analysis

"Strain gauges can also be used to pick up vibrational responses. A strain gauge is a metallic or semiconductor material that exhibits a change in electrical resistance when subjected to a strain. Strain gauges are constructed by bending a conducting wire back and forth in a serpentine fashion over a very small surface, which is then bonded to the device or structure to be measured. As the structure strains, the resistance of the serpentine wire changes. The gauge is made part of a Wheatstone bridge circuit, which is used to measure the resistance change of the gauge and hence the strain in the test specimen [see Figliola and Beasley (1991)]. Strain gauges are also used to form load cells" (Inman, 2014:590).

"*Strain gauges potentiometers as well as various optical, capacitive, and inductive transducers are often more suitable than accelerometers for low-frequency motion measurement*" (Inman, 2014:590).

3 Experimental modal analysis

3.1 Theoretical modal analysis of a beam

In order to simulate the operating environment of a ship, a free-free boundary condition was selected for the beam. According to beam theory, a free end of a beam is unrestricted in deflection and slope, but the shear force and bending moment becomes zero (Inman, 2014:547):

$$V(x) = EI\frac{d^3y}{dx^3} = 0 \quad \textbf{(16)}$$

$$M(x) = EI\frac{d^2y}{dx^2} = 0 \quad \textbf{(17)}$$

$$At\ x = 0, L \quad \textbf{(18)}$$

3.1.1 Natural frequencies and displacement mode shapes

Using Euler-Bernoulli beam theory, the following equations can be derived for natural frequencies and displacement mode shapes (DMS) (Inman, 2014:548).

$$\omega_n = \beta_n^2\sqrt{\frac{EI}{\rho A}} \quad \textbf{(19)}$$

$$f_n = \frac{\beta_n^2}{2\pi}\sqrt{\frac{EI}{\rho A}} \quad \textbf{(20)}$$

$$y_n(x) = a_1\sinh(\beta_n x) + a_2\sin(\beta_n x) + a_3\cosh(\beta_n x) + a_4\cos(\beta_n x) \quad \textbf{(21)}$$

Here the values for the four integration constants a_1, a_2, a_3, a_4 and β can be solved using the boundary conditions, yielding the following solution for a free-free beam (Inman, 2014:547 and Caresta, 2016). The theoretical DMSs obtained from Equation (23) are plotted in Figure 10.

$$\psi_n = \frac{\sin(\beta_n L) - \sinh(\beta_n L)}{\cosh(\beta_n L) - \cos(\beta_n L)} \quad \textbf{(22)}$$

$$y_n(x) = \sinh(\beta_n x) + \sin(\beta_n x) + \psi[\cosh(\beta_n x) + \cos(\beta_n x)] \quad \textbf{(23)}$$

Table 1: Separation constants of a free-free beam

Mode order *n*	$\beta_n L$
0	0 (rigid-body mode)
1	4.73004074
2	7.85320462
3	10.9956078
4	14.1371655
5	17.2787597

(Source: Inman, 2014:551)

3.1.2 Strain mode shapes

By differentiating the displacement mode shape, Equation (23), according to the Euler-Bernoulli beam theory relations and transforming according to the bending stress-strain relation, identified in Budynas and Nisbett (2015), the equation for the strain mode shape (SMS) can be obtained.

$$\theta_n(x) = \frac{dy}{dx} = \beta_n\{\cosh(\beta_n x) + \cos(\beta_n x) + \psi[\sinh(\beta_n x) - \sin(\beta_n x)]\}$$

(24)

$$\frac{M_n}{EI}(x) = \frac{d^2y}{dx^2} = \beta_n\{\sinh(\beta_n x) - \sin(\beta_n x) + \psi[\cosh(\beta_n x) - \cos(\beta_n x)]\}$$

(25)

$$\varepsilon_n(x) = \frac{d^2y}{dx^2} \times c = c\beta_n\{\sinh(\beta_n x) - \sin(\beta_n x) + \psi[\cosh(\beta_n x) - \cos(\beta_n x)]\}$$

(26)

The displacement and strain mode shapes are normalised to unity to display the relative shape of the modes. Figure 10 shows the first five theoretical DMSs and SMSs.

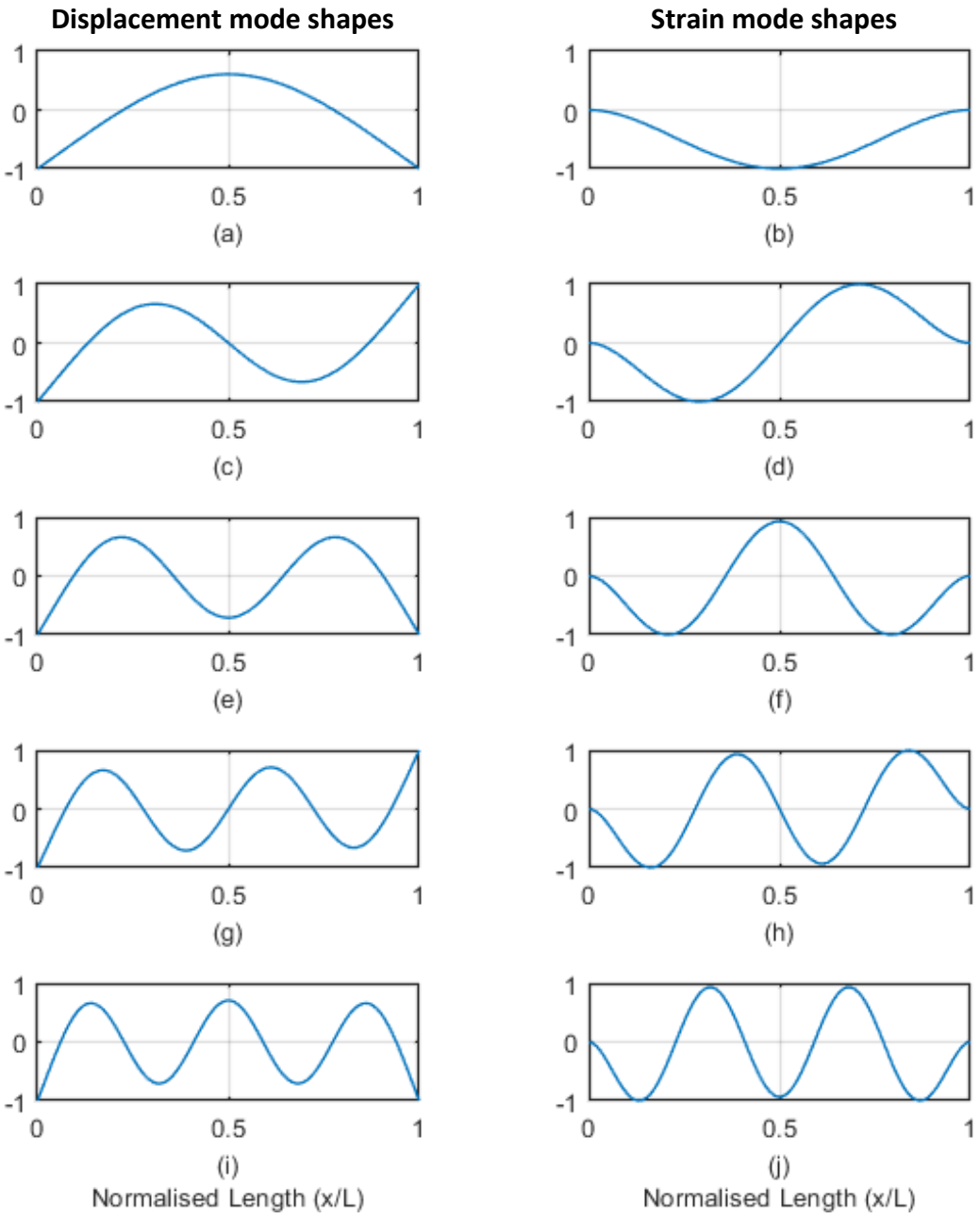

Figure 10: First five theoretical displacement and strain mode shapes of a free-free beam

3.1.3 Transforming mode shapes of a beam

Two methods will be explored for transforming experimentally determined displacement mode shapes to strain mode shapes. Considering that experimental data will be discrete and not continuous, the first method will employ numerical methods to numerically differentiate the data points obtained

that describe the displacement mode shape. The second method would fit Equation (21) to the data points and then differentiate the obtained curve in the continuous domain.

3.2 Experimental modal analysis experimental validation

3.2.1 Experiment aim

The experimental modal analysis (EMA) will attempt to obtain the beam's modal properties, specifically the natural frequencies, displacement and strain mode shapes. These experimentally determined modal properties will then be used to verify the results of the theoretical methods for determining displacement mode shapes and transforming them to strain mode shapes. In practice, one would also use the strain mode shapes obtained from this experiment to inform sensor placement for measuring operational loads. Since beams are such well known structures, the theoretical displacement and strain mode shapes are assumed to be accurate and will be used to inform sensor placement.

3.2.2 Experiment overview

This experiment will consist of both a classic displacement modal analysis with accelerometer measurements done concurrently with a strain modal analysis with strain gauge measurements. During this experiment, a shaker will be used to excite the beam by vibrating it at a range of frequencies.

3.2.3 Experiment setup

The experimental setup and rig are meant to be used for both the EMA experiment and cyclic loading experiment to follow. The experimental setup (seen in Figure 11) consists of a suspended beam, connected to a number of strain gauges and accelerometer sensor pairs. The beam is connected to a shaker that will be used to excite it at various frequencies. The modal hammer will be used to induce high frequency vibration in the beam during the cyclic loading experiments. The accelerometers, force transducer and modal hammer are connected to the data acquisition system (DAS) with coaxial cables that prevent the introduction of additional noise into the measurements. The strain gauges are connected to the DAS with multicore cables that is then connected to shielded multicore cables with 15 pin D-subminiature (D-sub) connectors. The shielded cables are then connected to the DAS. The use of D-sub connectors enables quick connection of strain gauge bridges to the DAS and moving the connected measuring point. This was needed since the laboratory only had a limited number of cables with the required connectors was available for use in all projects.

The DAS is then connected to a computer with an ethernet cable for the recording and analysing of the readings. The computer will use the DAS to generate the signal used by the shaker to excite the beam after the signal was amplified by the amplifier. The beam is suspended from a frame by bungee cord, in order to simulate a free-free boundary condition. The bungee cord simply slings around the beam, facilitating the movement of the rigid body mode. The shaker connects to the beam with a stinger to mitigate the effects of mass loading and the force changing direction when the beam deflects.

Since the same experimental rig will be used for the modal analysis and the cyclic loading experiments, it was decided to excite the beam at only one location with a shaker instead of a roving impact with a modal hammer. This setup enables the use of the shaker to induce cyclic loading in the beam for the cyclic loading experiments following the EMA experiment. The use of multiple measuring points provides spatial resolution for numeric differentiation when transforming experimental results.

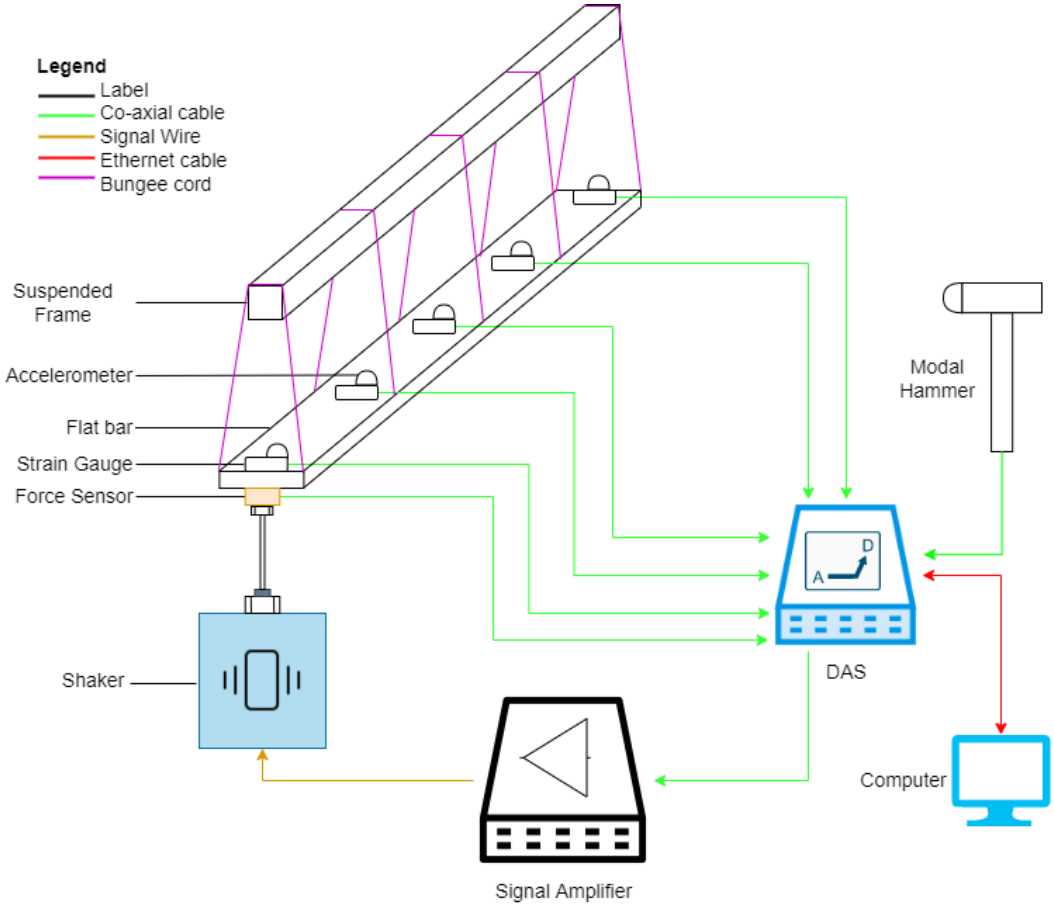

Figure 11: Illustrative experimental setup

3.2.4 Test sample

The test specimen is a simple flat bar beam with a 1600 mm x 40 mm x 4,5 mm profile, as is shown in Appendix B. The test specimen is made of commercial grade mild steel with a Young's modules of 200 GPa and density of 7800 kg/m^3. An I-beam was considered as the test specimen to better simulate the structural shapes used in ship structures. However, it was concluded that an I-beam would be too stiff for the equipment of the vibration laboratory to achieve significant strains in an I-beam for the cyclic loading experiments. Additionally, for the sake of simplification, the extra analysis and instrumentation required to determine and verify the location of maximum strain on an I-beam in bending, was concluded to be outside the immediate scope of this project when considering the project objectives.

By using the natural frequency equation shown in Equation (20) in Section 3.1.1, the natural frequencies displayed in Table 2 can be obtained for this test specimen. Calculations are included in Appendix A.

Table 2: First five theoretical natural frequencies

Natural frequency number	Frequency (Hz)
1	9.15
2	25.22
3	49.44
4	81.73
5	122.09

The first five mode shapes, as displayed in Figure 10, were also considered in the placement of sensors along the length of the test specimen as are indicated by the asterisks on Figure 33 and Figure 34 in Appendix A. It was decided to use seven evenly spaced sensor pairs, for both the modal analyses and cyclic loading measurements. The measuring points are indicated in Figure 12, with dimensions in mm. Strain gauges were stuck onto the indicated measuring points and accelerometers 15 mm offset towards the excitation location at Point 1, to prevent interference with the bridges. The shaker is attached at Point 1, a free end. This ensures that the beam is not excited on a node point that would have been stationary under true free-free boundary conditions, thus further decreasing the effect on the boundary conditions by the shaker.

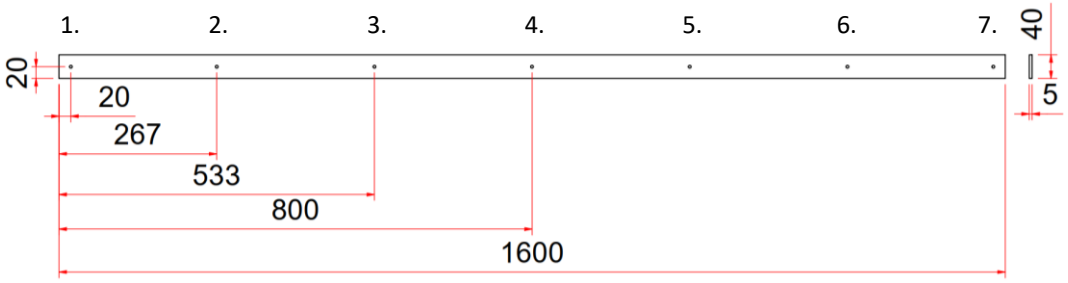

Figure 12: Measuring points on test specimen

3.2.5 Strain gauge configuration

A full bridge Type I strain gauge configuration was chosen for the strain measurements, as is shown in Figure 13. The wiring for this bridge configuration is shown in Figure 14. With the seven measuring points on the beam, this would result in 28 strain gauges bonded to the beam's surface.

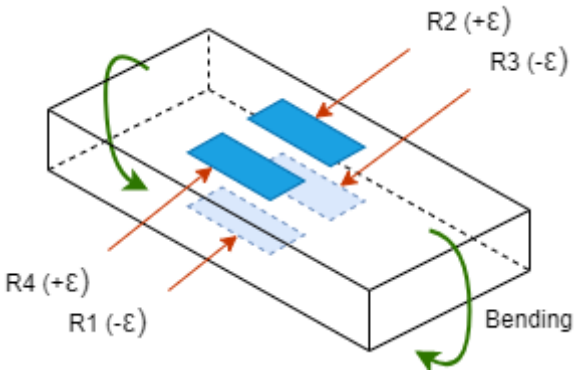

Figure 13: Full bridge type I

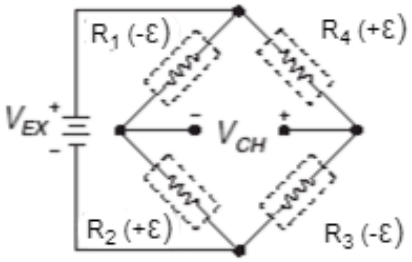

Figure 14: Full strain gauge bridge circuit diagram

(Source: Transducer Techniques, [s.a.])

This configuration only measures bending strain, ε_b, while cancelling out axial, ε_a, and thermal, ε_T, strain, as is shown in Equations (25) to (27) below. Another advantage of this bridge configuration is that it enables the use of common mode rejection, that reduces noise in the measured signal.

In the full bridge configuration, the measurement signal, V_{CH}, is carried on two wires to the DAS. This enables a differential input to be used where the measurement signal is superimposed on a common mode voltage equal to half the excitation voltage, V_{EX} (Siemens, 2019). This rejects the noise that would

have been introduced by the power supply. However, noise being induced in the wires is still a problem since wires of this length are susceptible to Electro-Magnetic Field (EMF) interference (Siemens, 2019).

The gauge factor (GF) is specific to each strain gauge, relating the change in resistance to change in strain and is around 2 for metallic strain gauges with a Poisson's ratio of about 0.3 (Figiola & Beasley, 2019).

$$\frac{dV_{CH}}{V_{EX}} = \frac{GF}{4}(\varepsilon_1 - \varepsilon_2 + \varepsilon_3 - \varepsilon_4) \quad \textbf{(27)}$$

$$\frac{dV_{CH}}{V_{EX}} = \frac{GF}{4}[(\varepsilon_a - \varepsilon_b + \varepsilon_T) - (\varepsilon_a + \varepsilon_b + \varepsilon_T) + (\varepsilon_a - \varepsilon_b + \varepsilon_T) - (\varepsilon_a + \varepsilon_b + \varepsilon_T)] \quad \textbf{(28)}$$

$$\frac{dV_{CH}}{V_{EX}} = -\frac{4 \cdot GF}{4} \cdot \varepsilon_b \quad \textbf{(29)}$$

3.2.6 Hardware specifications

The accelerometer is selected by considering the expected natural frequencies displayed in Table 2. The Pico Coulomb (PCB) 333B32 Integrated Circuit-Piezoelectric (ICP®) accelerometer, from PCB Piezotronics, with the specifications listed in Table 3, was available in the vibration laboratory for final year product experiments and will meet these requirements.

Table 3: PCB 333B32 ICP® accelerometer specifications

Category	Value
Sensitivity	(±10%)100 mV/g (10.2 mV/(m/s²))
Measurement Range	±50 g pk (±490 m/s² pk)
Broadband Resolution	0.00015 g rms (0.0015 m/s² rms)
Frequency Range	(±5%) 0.5 to 3000 Hz
Sensing Element	Ceramic
Mass	4.0 g

(Source: PCB Piezotronics, [s.a.] a)

The strain gauges chosen are 1-LY41-6/350 steel foil linear educational strain gauges from HBM with a resistance of 350 Ω ±0.3% and a GF of approximately 2 (HBM, [s.a.]).

The shaker selected is the Vibro PET-01 from IMV, with the specifications displayed in Table 4. This covers the first five natural frequencies that the author aims to verify in this study.

Table 4: IMV Vibro PET-01 shaker specifications

Category	Value
Frequency range	2 – 12 000 Hz
Rated sine force	9.8 N
Max. acceleration	490 m/s^2
Max displacement	5 mm (pk-pk)

(Source: IMV, [s.a.])

The force transducer between the stinger and the beam is a PCB 208C03 ICP® force transducer, the specifications of which are displayed in Table 5.

Table 5: PCB 208C03 ICP® force transducer specifications

Category	Value
Measurement Range	2.224 kN
Sensitivity	2248 mV/kN
Low Frequency Response	(±5%) 0.0003 Hz
Upper Frequency Limit	36000 Hz
Measurement Range	2.224 kN

(Source: PCB Piezotronics, [s.a.] b)

The modal hammer, with tip force sensor, that was chosen, is the PCB 086C01 ICP® Impact Hammer with the following specifications:

Table 6: PCB 086C01 ICP® impact hammer specifications

Category	Value
Sensitivity	11.2 mV/N
Measurement Range	±444 N pk
Hammer Mass	0.10 kg

(Source: PCB Piezotronics, [s.a.] c)

The data acquisition system (DAS) is a Siemens Signal Conditioning and Data Acquisition System (SCADAS) with a maximum acquisition rate of 204.8 kHz (Siemens, 2022). Considering that the highest natural frequency that is expected is 122.09 Hz, the minimum sample rate to prevent aliasing is twice that at 244.18 Hz. To provide a safety margin against aliasing of the measured signal, the

sample rate will be set to 500 Hz. This SCADAS Mobile consisted of an XSI card for shaker signal generation, a V8E for accelerometer measurements and a VB8E for strain gauges.

The computer was chosen according to the minimum system requirements of the DAS and data processing software. The software used for data acquisition, recording, processing and display is Siemens' Simcenter Test Lab. The software is needed to use the DAS and includes all the setup and calibration steps required for experimental modal analysis and measurements with the sensors of the experimental rig.

3.2.7 Experimental rig

The beam was cut to length by the M&M workshop. The measuring point surfaces were prepared and instrumented and the rig set up by the author.

The surface preparation of the beam included removing the oxidation scale that formed during the hot rolling process with sandpaper to expose the actual surface of the material for the strain gauges to be bonded to. The sandpaper was then gradually progressed to a finer grit up to a 320 grit to create a smooth surface without any possible stress concentrations. The exact measuring point and position of each strain gauge was then measured and marked with a ball point pen. The ball would leave a small indentation in the surface and it was thus important to mark the surface only next to where the strain gauge would be affixed. The surfaces were then cleaned thoroughly with acetone to remove oils, ink and particles. Acid was then used to etch the surface and alkaline was used to neutralise it again. The strain gauge was positioned along the measured point and held in place with cellotape while M-bond catalyst was applied to the bottom surface of the strain gauge. The gauge was then bonded to the surface by sticking it with Z 70 Schnellklebstoff glue from HBM. Only a small amount of glue and catalyst was applied and then pressed for two minutes by the author's finger to ensure that there is only a small amount of glue between the gauge and beam surface. After a minimum of 10 minutes the cellotape was removed and the quality of the bond visually inspected.

Solder pads were added to both sides of the beam to prevent vibration in the bridge wires from affecting the strain readings measured by the gauges. The bridges were wired according to the circuit diagram in Figure 14. Accelerometers were stuck to the surface of the beam using super glue. The accelerometers would therefore only measure accelerations normal to the surface of the beam. It is, however, assumed that the accelerometers always measure in the y-direction and that the change deviance from the actual y-direction acceleration measurement is negligible. A fully instrumented measuring point is shown in Figure 15 (a) and (b).

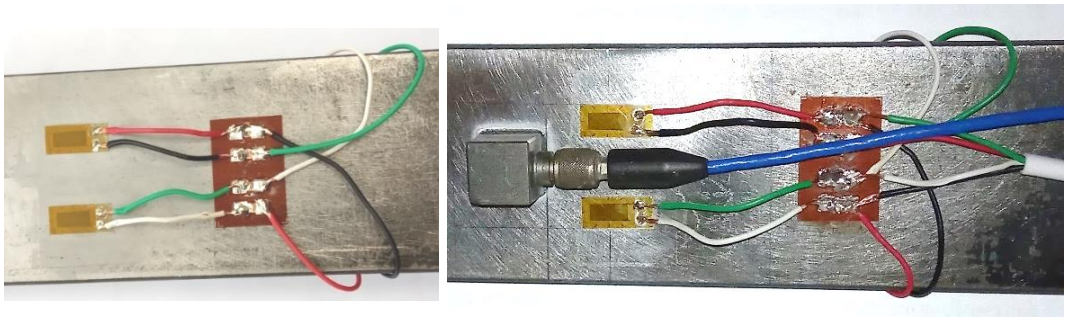

(a) (b)

Figure 15: Top (a) and bottom (b) of a measuring point

At this stage, the full experimental rig could be set up. At first, the beam was suspended with bungee cord, but due to the beam's small mass, the bungee cord was found to be too stiff and rubber bands were then used to simulate the free-free boundary condition. The shaker was bolted to a heavy channel section base to ensure that it would not move during beam excitation. The fully set up experimental rig is shown in Figure 16. The beam's height was adjusted so that it was at the same level as the mounting stud adapter, the beam checked with a spirit level to be horizontal, and finally stinger alignment was checked before connecting the beam and the shaker.

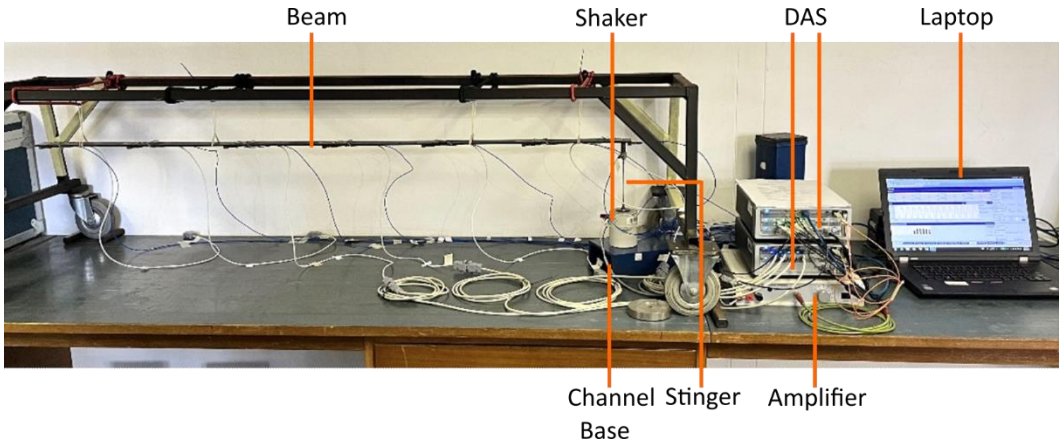

Figure 16: Implemented test set up

Unfortunately, an adapter was required to act as the mounting stud of the force transducer. Since this adapter consisted of a short steel rod with a threaded tip on one end and a threaded hole on the other, it added significant mass to the one end of the beam, altering its boundary condition and mass characteristics. A close-up view of the shaker-beam connection through the stinger and force

transducer with the adapter mounting stud at Measuring Point 1 is shown in Figure 17.

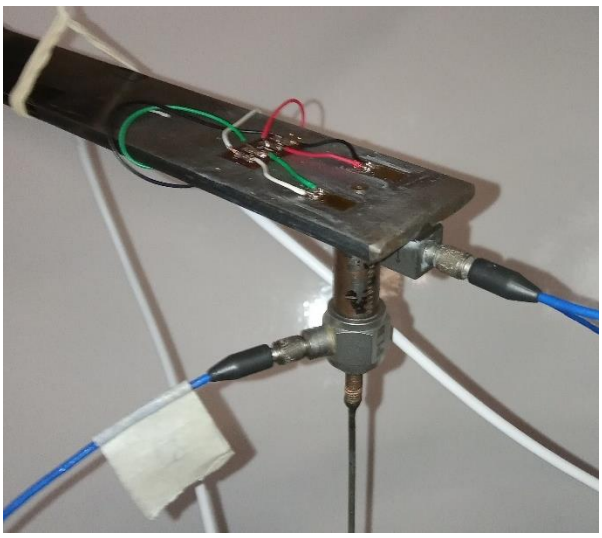

Figure 17: Shaker-beam connection

3.2.8 Experimental modal analysis steps

The abbreviated overview of the experimental procedure for the EMA is shown in Figure 18. The data analysis will be discussed in Section 3.3.

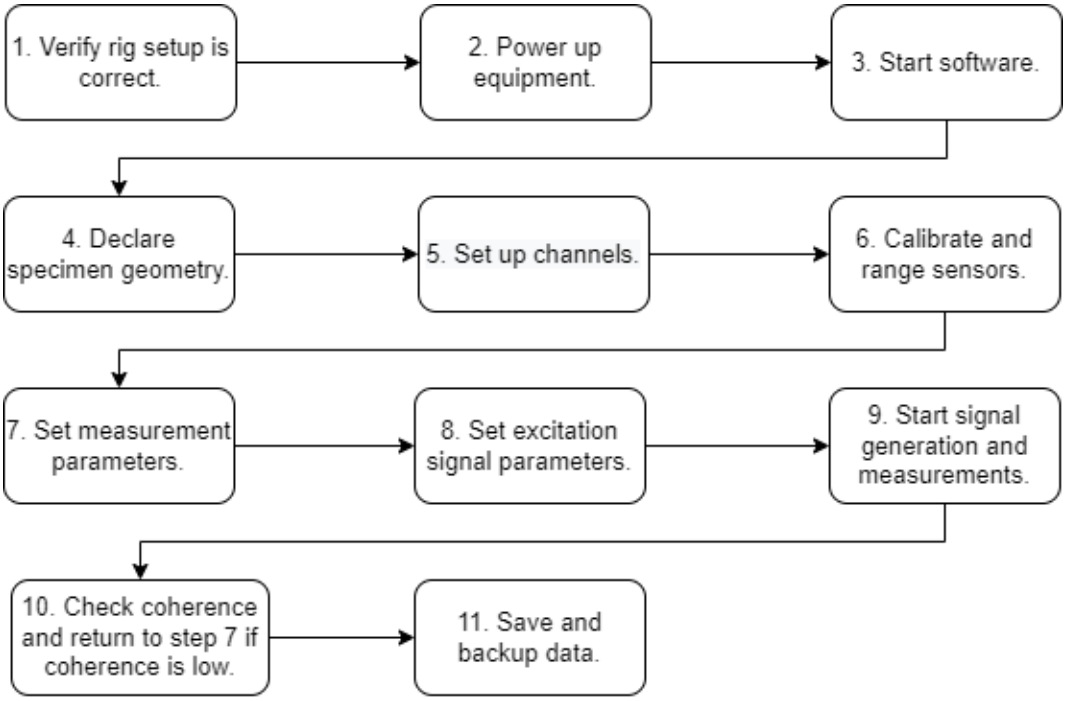

Figure 18: EMA steps

First the experimental rig setup is checked to verify that all components are set up and connected according to the planned setup. Then all the equipment is powered on and the Siemens Simcenter Testlab software is started. From this stage all the measurement and excitation setup steps are conducted in the Testlab software as well as the testing activation and the majority of the modal data analysis. The remainder of the EMA data analysis and data set transformation was done in MATLAB. The specimen geometry is declared. Channels are set up, by declaring the sensor specifications for each channel and allocating each sensor to a measuring point on the specimen geometry as well as the measuring direction. The strain gauge bridges must be nulled (zeroed) and the calibration verified using the software. The sensors and amplifiers are then ranged by exciting the system at conditions similar to the test conditions and setting the rail (saturation) voltages to prevent overloading of the system, clipping of signals, and ensuring that the amplifier gain of the measurement signals is high enough to produce reliable data. Thereafter, the measurement and excitation parameters are declared. These parameters are displayed in Table 7 below.

Table 7: EMA measurement and excitation parameters

Parameter	Value
Spectral lines	2048
Resolution	0.25 Hz
Bandwidth	250 Hz
Sample rate	500 Hz
Sample period	0.0020 s
Window acquisition time	8 s
Window type	Hanning
Excitation signal type	Burst random
Burst time	50 %
Burst ramp time	0.250 s
Averages	25

After the measurement and excitation parameters have been set, the test can be run up to 25 times to obtain 25 different FRFs for each measuring point, that will be averaged for use in the modal data analysis. The test is repeated with the cables moved so that the strain gauges that were previously disconnected are now connected. After the average from the 25 tests has been obtained for each measuring point with all sensors, the average coherence is checked to ensure that it is at one for the vast majority of frequencies on the averaged FRF. Dips in coherence can be expected at resonance (natural frequency) and antiresonance points, due to leakage. This can be mitigated by setting up an excitation signal with a periodic nature that matches the measuring window. If the coherence is acceptable, the researcher can proceed to data analysis.

For the case of the author's EMA experiments, a periodic chirp excitation signal achieved coherence at unity over the majority of the bandwidth and at resonance points, except at the low and high frequency ends of the measured bandwidth. This proved to be unacceptable, since this causes low coherence at and around the first expected natural frequency. Using a bust random signal provided a coherence that was acceptable, but the excitation signal's periodic burst parameters were not ideal, thus not eliminating dips in coherence at resonance points.

3.2.9 Expected results

The expected natural frequencies are displayed in Table 2 and the expected normalised displacement and strain mode shapes in Figure 10.

3.3 Experimental modal data analysis

3.3.1 Displacement modal analysis from acceleration measurements

To conduct the displacement modal analysis, the natural frequencies and damping ratios need to be determined first, using the acceleration measurements. Using the obtained average FRF for the whole structure, Siemens Simcenter Testlab calculates different poles for each possible resonant point on the FRF, with its frequency and damping ratio. This should be done after the order of the solution to be calculated, is set. The user then needs to select a pole that is indicated to be stable by the software and which the user can see does not change much at higher orders. The user must also use his/her discretion in determining if a peak on the FRF, that has poles calculated for it, is indeed a resonance point or, for example, just electrical noise. The results is shown in Table 8.

After this, the displacement mode shapes are determined. The acceleration data sets are selected and Testlab determines the DMSs that correspond to each natural frequency. The user needs to check that each mode shape makes sense, especially considering that there is a well-established model for this structure at the boundary conditions that is being simulated. In the case of the author's experiments, at this stage it was found that the accelerometer that was initially used at Measuring Point 3 was faulty, giving measurements in the wrong direction and magnitude. Results obtained with a different accelerometer matched the expected results as is shown in Figure 19, indicated by the orange asterisks on the expected theoretical DMSs.

3.3.2 Strain modal analysis from strain measurements

The strain modal data analysis consists of the same steps as the displacement modal data analysis, but using the strain frequency response instead of the acceleration frequency response and selecting strain measurements and FRFs from the two identical tests, to include strain measurements from all the measuring points are included. Results for natural frequencies included in Table 8 and mode shapes in Figure 19 are indicated by the orange asterisks on the expected theoretical SMSs.

3.3.3 Strain modal analysis from acceleration measurements

For transforming experimental displacement mode shapes to strain mode shapes, the curve fitting methods tested proved unreliable. Non-trigonometric functions, such as polynomials, have the problem that after differentiation its shape would be completely different from the desired strain mode shape. Low order piecewise functions could become discontinuous after differentiation. For these reasons, Equation (21) proved to be suitable for this application. The curve fitting method proved to be ineffective at higher order modes, since the fitting function would generate constants that fit Equation (21) to the average of the data points. Further exploration of curve fitting methods would be necessary to determine viability for this method for transforming mode shapes.

Numerical differentiation proved to have usable results. By using a two-point forward difference numerical differentiation formula and differentiating the theoretical and experimental DMSs twice numerically, discrete points were obtained that closely approximated the theoretical strain mode shape. The results of this method is shown in Figure 21. It was necessary to only use a point difference formula that is as small as possible, due to the low spatial resolution. Three-point forward and four-point central difference formulas would give results that averaged the shape of the function. The two-point difference formula used is shown in Equation (30) below. By using this method, the number of data points would decrease with each differentiation, but since both theory and experimental data indicate that the strain at a free end of a beam is zero, the strain at the free ends of the transformed mode shapes were set to be equal to zero. Sample calculation code is shown in Appendix A.2, where the same transformation is conducted on a similar data set, but without the normalisation step.

$$f'(x_i) = \frac{f(x_{i+1}) - f(x_i)}{x_{i+1} - x_i} \qquad \textbf{(30)}$$

3.4 Discussion of experimental modal analysis results

The experimental natural frequencies and damping ratios with the theoretical natural frequencies, are displayed in Table 8. Due to the 0.25 Hz FRF resolution, the experimental frequencies are not reported below the decimal.

Table 8: EMA resulting natural frequencies

Mode order	Theoretical (Hz)	Displacement modal analysis (Hz)	Displacement damping ratio (%)	Strain modal analysis (Hz)	Strain damping ratio (%)
1	9.150	9	1.00	9	0.73
2	25.22	25	0.41	25	0.47
3	49.44	49	0.30	49	0.29
4	81.73	81	0.21	81	0.22
5	122.09	120	0.15	120	0.16

From these results it is shown that the displacement modal analysis using the acceleration frequency response and the strain modal analysis using the strain frequency response, yielded the same experimental natural frequencies. It also shows that the theoretical and experimental natural frequencies match each other, with a maximum difference of 0.73 Hz (0.9 %) in the first four modes and 2.09 Hz (1.7 %) at the 5^{th} mode. It can also be seen that the experimental damping ratios decrease as the natural frequencies increase. This indicates that lower frequency vibrations in the structure will attenuate quicker, as can be expected for a structure of this type and material. These results verify the theoretical methods used for determining natural frequencies and that this experimental setup is well suited to simulate a free-free beam.

The normalised experimental mode shapes is shown in Figure 19, indicated by orange asterisks for each measuring point, overlaid on the theoretical mode shapes indicated by the continuous blue line. From these results it is shown that the experimental DMSs closely resemble the general shape of the theoretical DMSs. However, there are difference in amplitude, especially at the accelerometers at Measuring Point 2, 4 and 5. This indicates that these accelerometers are in need of recalibration. Unfortunately, the author realised this only during data analysis, after both the modal analysis experiments and cyclic loading experiments were completed. The results displayed in Figure 19 do however correlate well with the theoretical methods used, verifying those methods to be viable for a known structure, well modelled structure, such as this free-free beam.

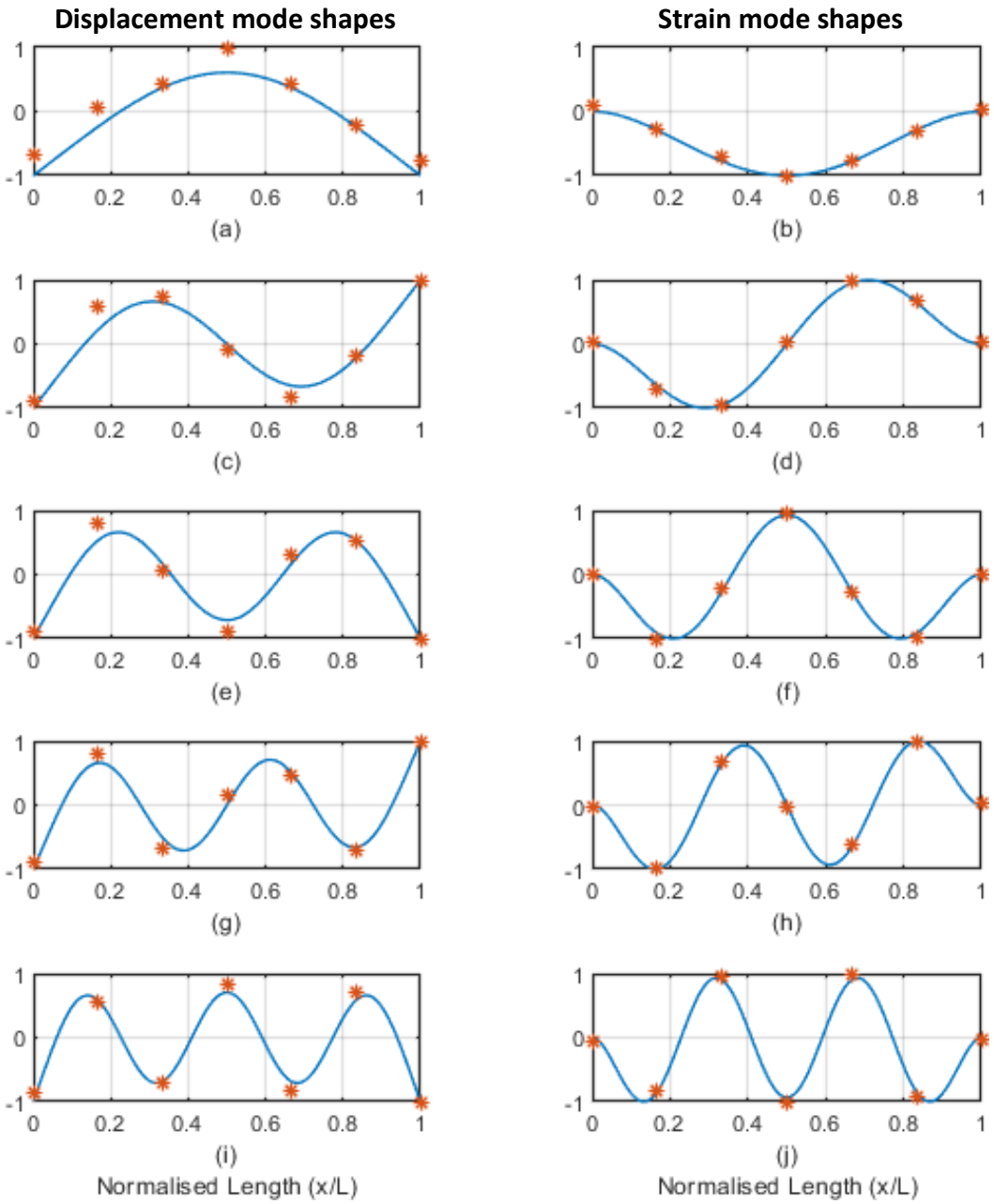

Figure 19: Experimental mode shapes in orange

The modal assurance criterion (MAC) generated using Simcenter Testlab compares the different experimental mode shapes and shows that the experimental DMSs and experimental SMSs are indeed unique. This is shown in Figure 20.

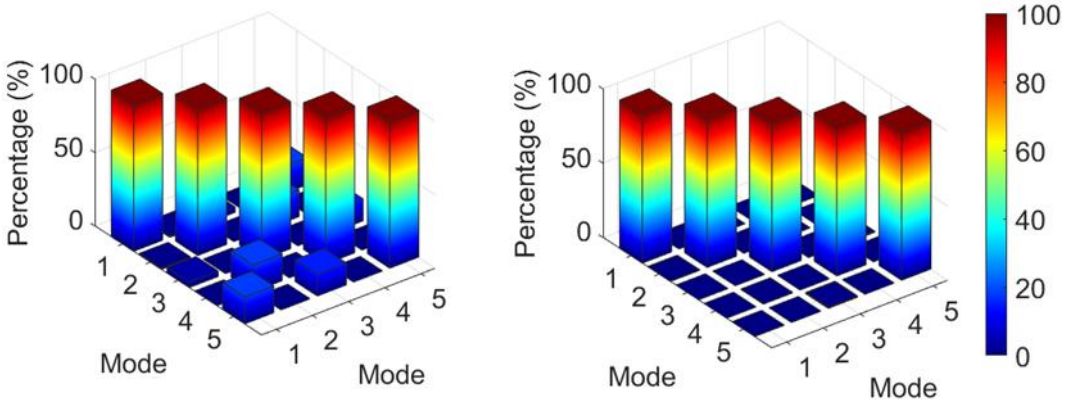

(a) (b)

Figure 20: Displacement (a) and strain (b) EMA modal assurance criterion

The results of the transformed SMSs is shown in Figure 21. First, seven discrete points were declared on the theoretical displacement mode shape and transformed to strain to test the transformation method. These yielded accurate results, although not exactly the same as the theoretical SMS and is shown as blue circles in Figure 21. Then the experimental DMSs' data points were transformed to strain. These results is shown as orange asterisks in Figure 21. The correlation between the strain mode shapes obtained by transforming acceleration mode shapes to those experimentally obtained from strain measurements is displayed in Table 9. For the higher modes, these transformed SMSs were fairly accurate, yielding correlations of 96.87 % and higher. However, transformed SMS 1 proved to be very inaccurate, showing a correlation of only 51.29 %. This indicates that the numerical differentiation transformation method is especially sensitive to changes in the sign of a gradient's derivative, as is the case of the DMS data points of Mode 1. This was likely caused by inaccurate sensitivity values, since it appears that the accelerometer manufacturer calibration sheets are no longer accurate. In hindsight, the author could have compared the readings of the accelerometers utilised in the test rig before affixing them.

Table 9: Transformed and experimental SMS correlation

Mode order	Correlation (%)
1	51.29
2	96.87
3	98.62
4	99.26
5	99.80

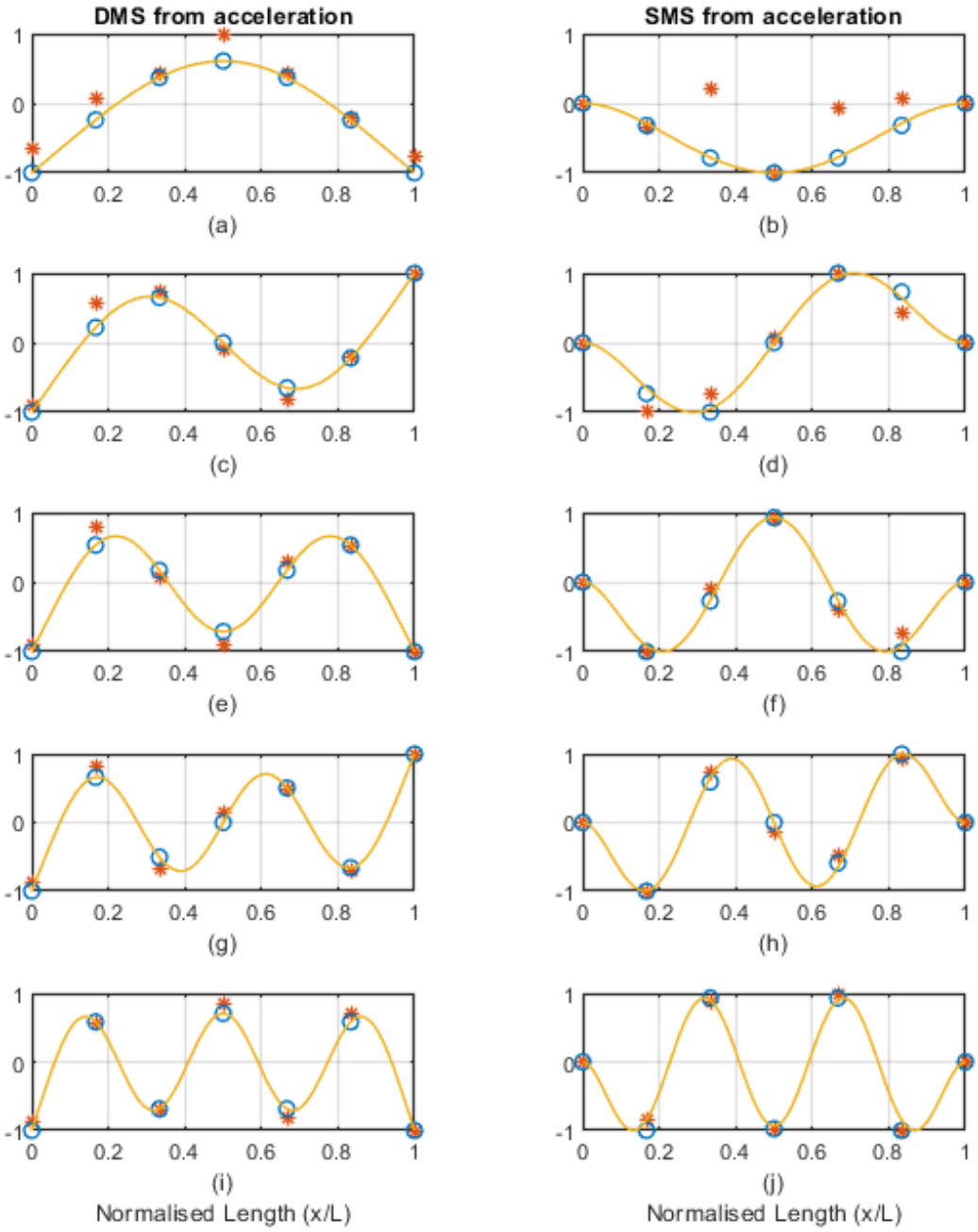

Figure 21: Transformed strain mode shapes

Data relating to acceleration DMSs displayed as orange asterisks. Data relating to theoretical DMSs displayed as blue circles. Theoretical continuous DMSs and SMSs in yellow.

4 Fatigue life analysis

Traditionally, accumulated fatigue damage and fatigue life estimates for operational structures were determined by taking strain measurements, conducting rainflow load cycle counting and then applying Palmgren-Miner's method, as discussed in Section 4.1.1.

4.1 Theoretical fatigue life analysis

4.1.1 Fatigue damage and life estimates from strain

To obtain a fatigue life estimate, Wöhler SN curves, Palmgren-Miner's method and linear damage accumulation are used. First the strain measurements are converted to stress by simply multiplying it with Young's modulus, per the relation shown in Equation (7).

When using actual load histories, a form of cycle counting needs to be employed to determine the stress ranges and number of cycles counted for each stress range, to then make use of Palmgren-Miner's method and linear damage accumulation. Rainflow counting, as prescribed by ASTM E1049-85, is one such a standardised cycle counting method for use in fatigue analysis.

When the stress ranges and cycle counts have been obtained, the damage number can be calculated for each stress range with Equation (14). After this, the damage accumulation is calculated by summing all the damage numbers.

4.1.2 Fatigue damage and life estimates from acceleration

To apply Palmgren-Miner's method and linear damage accumulation, acceleration needs to be transformed to stress. First acceleration, $\ddot{y}(x,t)$, is integrated in terms of time, t, to velocity, $\dot{y}(x,t)$, and then again to displacement, $y(x,t)$ (Hibbeler, 2017).

$$\ddot{y}(x,t) = \frac{\delta^2 y(x,t)}{\delta t^2} \quad \textbf{(31)}$$

$$\dot{y}(x,t) = \frac{\delta y(x,t)}{\delta t} = \int_{\dot{y}_1}^{\dot{y}_2} d\dot{y} = \int_{t_1}^{t_2} \ddot{y}(x,t)\, dt \quad \textbf{(32)}$$

$$y(x,t) = f(x,t) = \int_{y_1}^{y_2} dy = \int_{t_1}^{t_2} \dot{y}(x,t) dt \quad \textbf{(33)}$$

Differentiate in position, x:

$$y = f(x,t) \quad \textbf{(34)}$$

$$\frac{\delta y(x,t)}{\delta x} = \theta(x,t) \quad \textbf{(35)}$$

$$\frac{\delta^2 y(x,t)}{\delta x^2} = \frac{M(x,t)}{EI} \quad \textbf{(36)}$$

Transform to strain, $\varepsilon(x,t)$:

$$\varepsilon(x,t) = -\frac{\delta^2 y(x,t)}{\delta x^2} \times c \quad \textbf{(37)}$$

Transform to stress, $\sigma(x,t)$:

$$\sigma(x,t) = -\frac{\delta^2 y(x,t)}{\delta x^2} \times E \times c \quad \textbf{(38)}$$

The method specified in Section 4.1.1 can be applied to determine the fatigue life estimate and linear damage accumulation. When working with measurement data sets, those data points will be discrete and thus numerical integration and differentiation is required.

4.2 Fatigue life analysis experimental validation

4.2.1 Experiment aim

The aim of the cyclic loading experiment is to generate measurement data sets that can be used to demonstrate, compare and evaluate the fatigue life estimate

and linear damage accumulation methods laid out in Section 4.1 for using both strain gauge and accelerometer measurements.

4.2.2 Experiment overview

The cyclic loading experiment will make use of the shaker to excite the free-free beam at a low frequency to induce cyclic loading in the structure. A modal hammer will then be used to impact the structure in order to induce high frequency vibration on top of the low frequency vibration. The low frequency will simulate the hogging and sagging of a ship and the high frequency will simulate wave slamming due to wave impacts. Both acceleration and strain measurements will then be used to calculate the stress in the structure and to determine a linear damage accumulation number and a remaining fatigue life estimate of the beam at the measured stress conditions.

4.2.3 Experiment setup

The same experimental setup and rig will be used as the one specified in Sections 3.2.3 to 3.2.7. The shaker enables the beam to be excited at a steady, low frequency. Multiple accelerometers are needed to provide spatial resolution when performing numeric differentiation to transform displacement to stress. Strain gauges positioned at the same measuring points will then be used to verify the transformed strain measurements obtained from the transformed acceleration data.

4.2.4 Experimental fatigue life analysis steps

The abbreviated overview of the experimental procedure for the fatigue analysis consists of the steps shown in Figure 22.

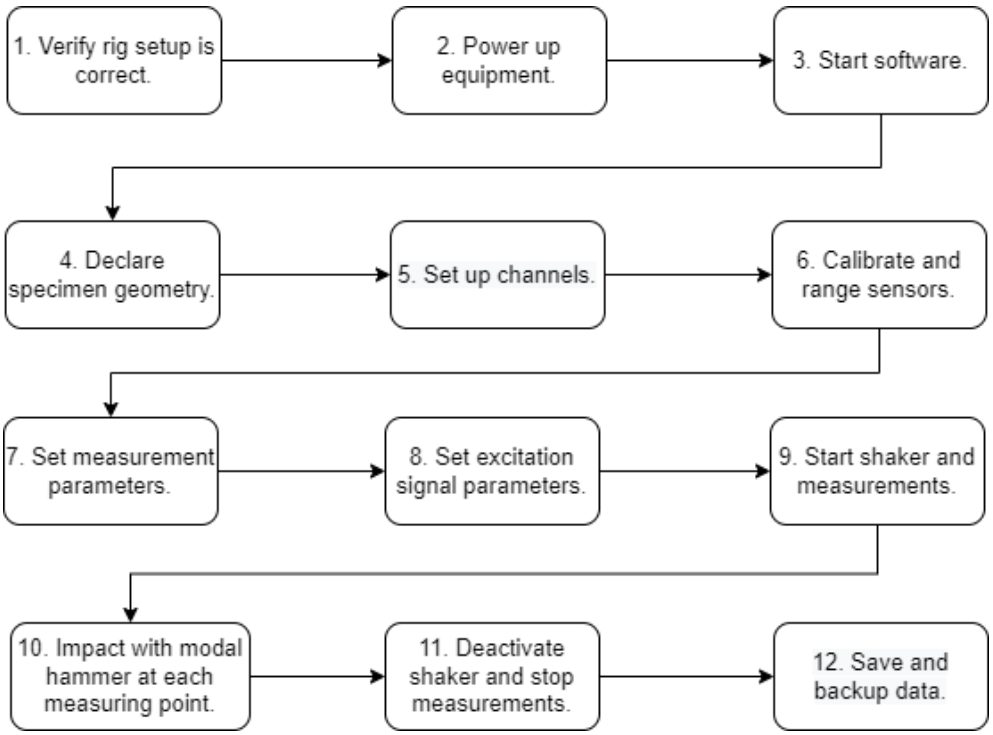

Figure 22: Cyclic loading experiment steps

When conducted from scratch, the initial setup steps are similar to those of the EMA experiment up to the strain gauge nulling and calibration verification step. First the experimental rig setup is checked to verify that all components are set up and connected according to the planned setup. Then all the equipment is powered on and the Siemens Simcenter Testlab software is started. The specimen geometry is declared. Channels are set up by declaring the sensor specifications for each channel and allocating each sensor to a measuring point on the specimen geometry as well as the measuring direction. The strain gauge bridges must be nulled and the calibration verified using the software.

The sensors and amplifiers are then ranged by exciting the system at conditions similar to the test conditions, at a steady low frequency and with high frequency components added by modal hammer impacts. The ranging is done by setting the rail voltages to prevent overloading of the system, clipping of signals, and ensuring that the amplifier gain of the measurement signals is high enough to produce reliable data. During this stage it is especially important to pay attention to stinger alignment and shaker displacement amplitude. A displacement amplitude as large as possible is desired, but not to such a degree that the beam oscillates beyond the full range of the shaker. When this occurs, the beam will start to tug on the shaker and introduce asymmetric cyclic loads during the steady period of excitation. Poor stinger alignment will cause excessive axial displacement of the beam during excitation.

After this, the low frequency excitation and measurement parameters are set for the shaker and sensors. The sampling rate was set to 5120 Hz. First a noise floor measurement is taken where no input is given to the shaker and the beam is not excited. This is to determine the base noise level that will be present in measurement signals. Then the beam is excited using only the shaker to induce a low frequency vibration in the beam at 7 Hz. The 7 Hz frequency was chosen since it is close to the first (lowest) natural frequency and would thus be capable of causing large displacements and large strains. During this run, a rough measurement of the beam displacement amplitude is taken recording a video of the beam at Measuring Point 4 with a ruler in the frame. This rough displacement measurement can be used to conduct a sanity check on displacement values obtained from transformed acceleration measurements. The beam is then again excited at 7 Hz and the beam is impacted with the modal hammer at each measuring point. By changing the test in this way with each run, levels of complexity are steadily introduced into the measurements. This experiment was repeated four times at these conditions. The same experiment was conducted at higher frequencies and at different displacement amplitudes.

4.2.5 Expected results from strain measurements

Results from calculations using strain gauge measurements are expected to be realistic since only a scaling factor needs to be applied to attain stress from the readings, unlike the acceleration measurements which require intensive data processing to obtain stress values.

The strain gauge measurements were expected to show a higher level of noise in its measurements due to the lack of shielding of the cables connecting the bridges to the seven-core shielded cables. Due to the fact that the cables connecting the bridges to the shielded cable also does not consist of twisted pairs, the signals conducted by it will add interference to other signals conducted by it. Another possible cause of noise is poor strain gauge bonding to the metal surface, but poor bonding should be clearly visible in strain measurements.

4.2.6 Expected results from acceleration measurements

Results obtained from the accelerometer measurements were not expected to be highly accurate, but to be representative of actual experimental displacement and strain cases. The sensitivity of the differentiation to high frequency low amplitude noise and error accumulation caused by integration over long time ranges, are expected to be problematic (Figliola & Beasley, 2019:440). Another characteristic of the experimental measurements that could pose a challenge is the fact that these motions oscillate about a resting position and does not displace continuously in one direction.

4.3 Experimental fatigue life data analysis

MATLAB was used to develop the fatigue damage and life estimation algorithm discussed in this section. Sample code of the algorithm is shown in Appendix A.2.

4.3.1 Fatigue damage and life estimate from strain measurements

In the noise floor measurement and at lower altitudes the strain data was found to be especially noisy around 0 Hz, the 50 Hz of the local electrical grid and its harmonics. To mitigate the noise identified, a comb notch (band stop) filter was designed and implemented on the strain measurements. The noise floor before and after filtering is shown in Figure 23 for strain measurements at Point 4.

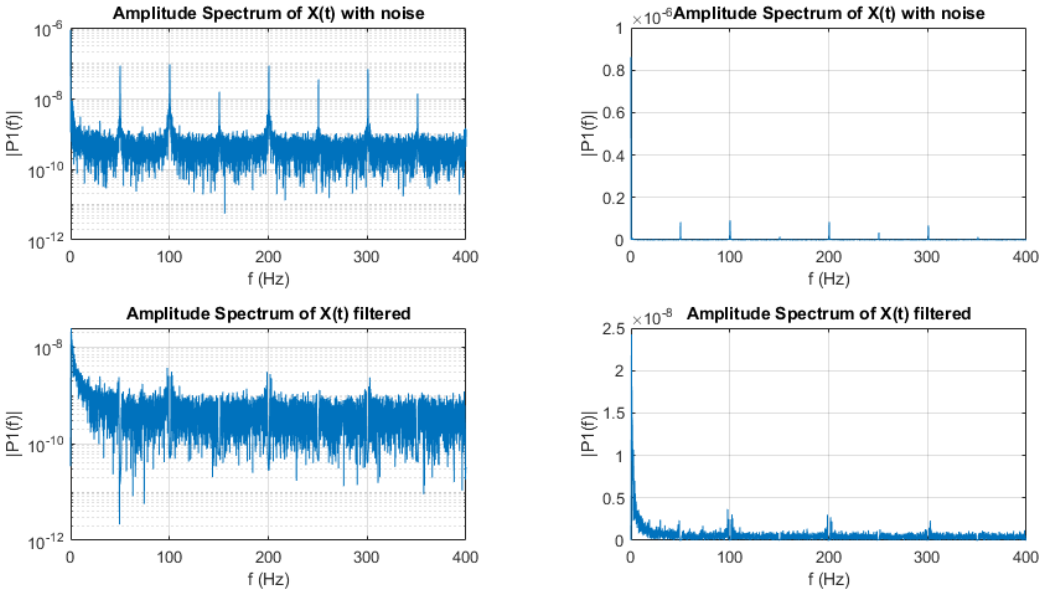

Figure 23: FFT of unfiltered (top left) and filtered noise floor measurement of strain gauge bridge at Measuring Point 4

After noise was filtered, the strain measurements were transformed to stress and the stress ranges and their cycle counts were determined using the MATLAB rainflow function. The commercial mild steel of the test specimen was assumed to have a SN curve similar to 1045 plain carbon (mild) steel that was hot rolled and normalised. Using the SN curve parameters found in Budynas and Nisbett (2015) for 1045 plain carbon steel, a piecewise SN curve function was developed using Equation (12). The result is shown in Figure 35 in Appendix A.2. Using this piecewise function, the number of cycles to failure, N, at each stress range and the individual damage number for that stress range was calculated using Equation (14) and its cycle counts. Finally, the accumulated damage was

calculated for the test run by summing the damage numbers for each stress range.

4.3.2 Fatigue damage and life estimate from acceleration measurements

For the fatigue calculations from acceleration measurements, the acceleration data for each measuring point was first transformed individually. A second order high pass Butterworth filter with a cutoff frequency of 0.5 Hz is applied to prevent drift of the integral results. Fortunately, the noise floor for the acceleration measurements was insignificant in comparison to the amplitude of the accelerations measured. Then the acceleration data sets are integrated numerically using the MATLAB cumtrapz function, that employs cumulative trapezoidal numerical integration with the time step dt being equal to the sample period of 195.3125 µs. After the first integration, the velocity data set is detrended with the MATLAB detrend function to remove any polynomial trends and ensure that the final integral oscillates around the 0 m initial position. A final numerical integration is done on the detrended velocity data set to obtain the displacement at each measuring point. An example of the results obtained from the integration process is shown in Figure 24 for an example 7 Hz sine wave digitally generated test set.

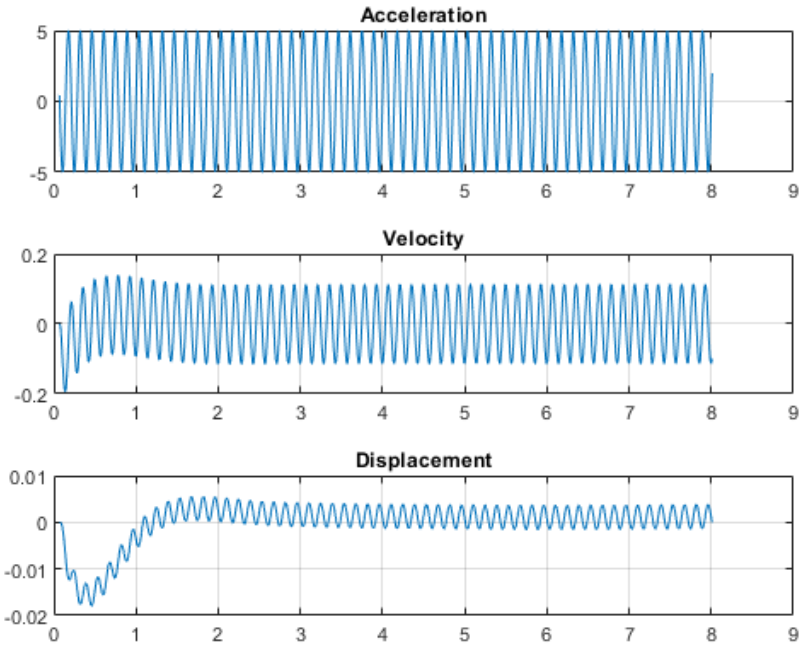

Figure 24: Acceleration to displacement transform example results

Unfortunately, this method does not yield realistic displacement results, since it indicates that the beam oscillates at a far offset position during the first second and then oscillates around a position slightly offset from zero for the majority of the test data set. However, basic differential characteristics do hold true, i.e. the differential of a peak turning point is zero at that time instance and the second derivative is negative. This relation is shown in Figure 36 in Appendix A.2 for a 7 Hz low frequency run.

At this stage all the displacement measurements over the whole beam are considered at each time instance to form a spatial representation of the beam. This displacement curve of the beam is then numerically differentiated twice, with the two-point difference formula in Equation (30), to transform the displacement beam shape to a strain curve. This is the same method employed in the EMA data processing to transform DMSs to SMSs, without the normalisation to unity step. An example of the final and intermediate results obtained from this method is shown in Figure 25 for an example displacement curve, compared to the strain data obtained. This transformation process yields realistic results, as was demonstrated by the DMS transformation results in Section 3.4.

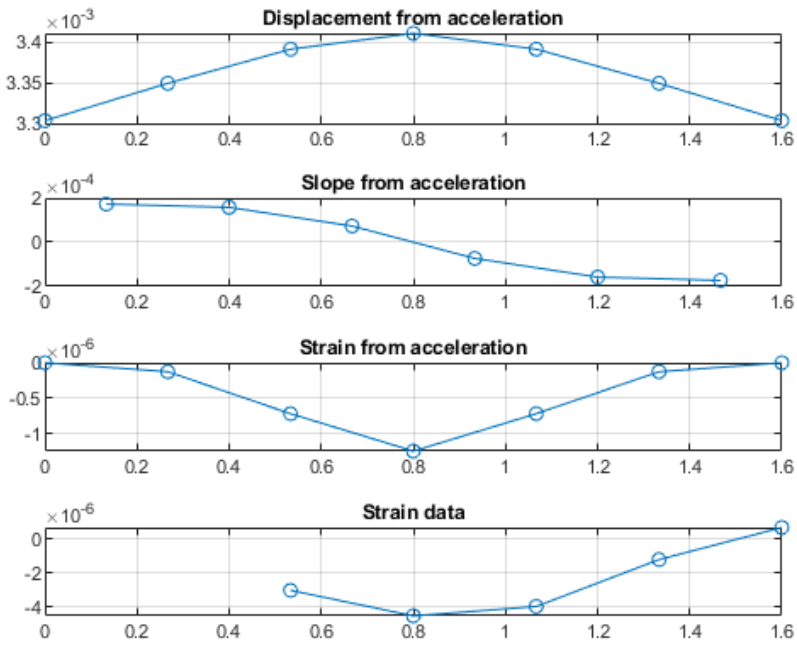

Figure 25: Displacement to strain transform example results

When the transformed strain data set has been obtained, the same algorithm laid out in Section 4.3.1 for actual strain data sets can be employed to determine accumulated fatigue damage.

4.4 Discussion of fatigue life analysis results

4.4.1 Low frequency experiment results

For the first test case where the beam was only excited with a 7 Hz low frequency, the aim was to acquire symmetric acceleration cycles. To achieve this, the optimal displacement range of the shaker was prioritised. This allowed for the capture of a data set where the beam did not tug on the shaker and acceleration cycles would be symmetric. The resulting steady acceleration measured at Measuring Point 4 was 3.5 m/s^2. The results of the acceleration to displacement transform for Measuring Point 4 is shown in Figure 26. These results seem reasonable and realistic for the majority of the time range, and they pass the sanity check since rough visual measurements indicated that for this test case, the displacement amplitude at Point 4 was about 3 mm. These displacements of about 3 mm would prove to be too small to cause damaging strain in the beam.

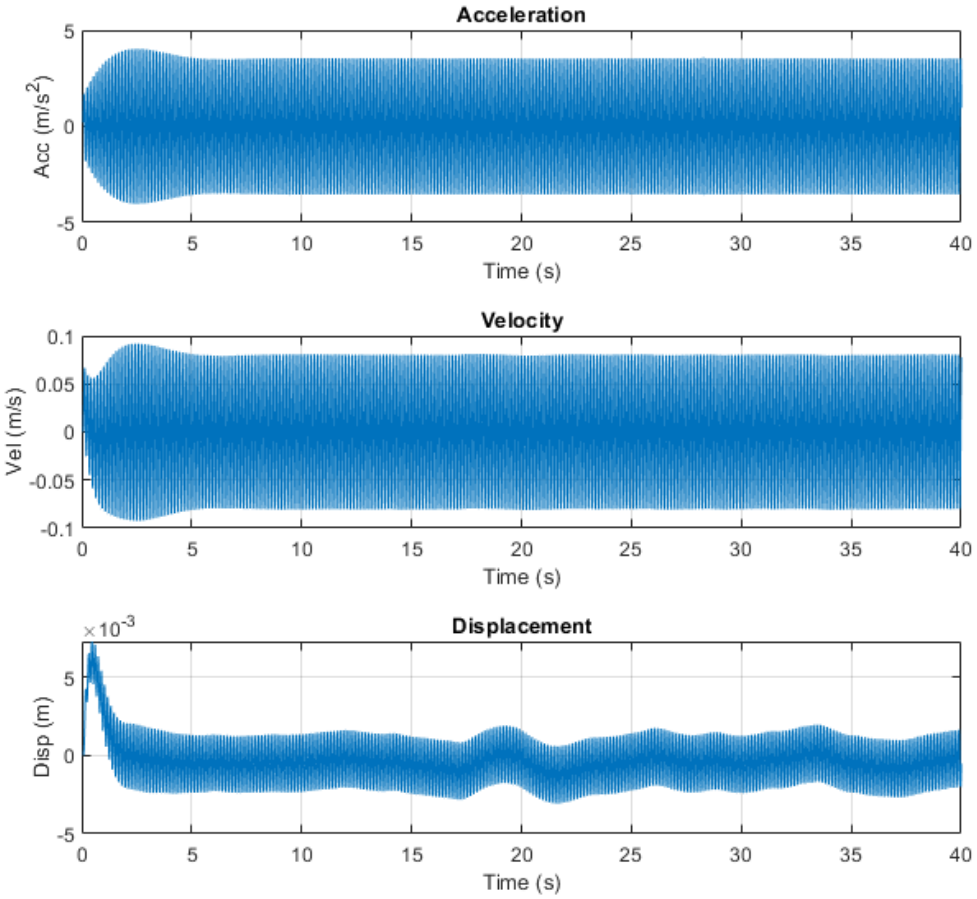

Figure 26: Low frequency experimental acceleration to displacement transform results

The motivation for having symmetric cyclic acceleration measurements at each measuring point was that the expectation that this would create a data set would yield transformed displacement and strain curve results that portray a realistic representation of the beam's actual experimental conditions. However, during this stage of the cyclic loading data analysis it became apparent that the accelerometers' manufacturer calibration certificates needed to be verified. This was due to the poor level of symmetry in the resulting displacement shape shown in Figure 27 – displacement from acceleration.

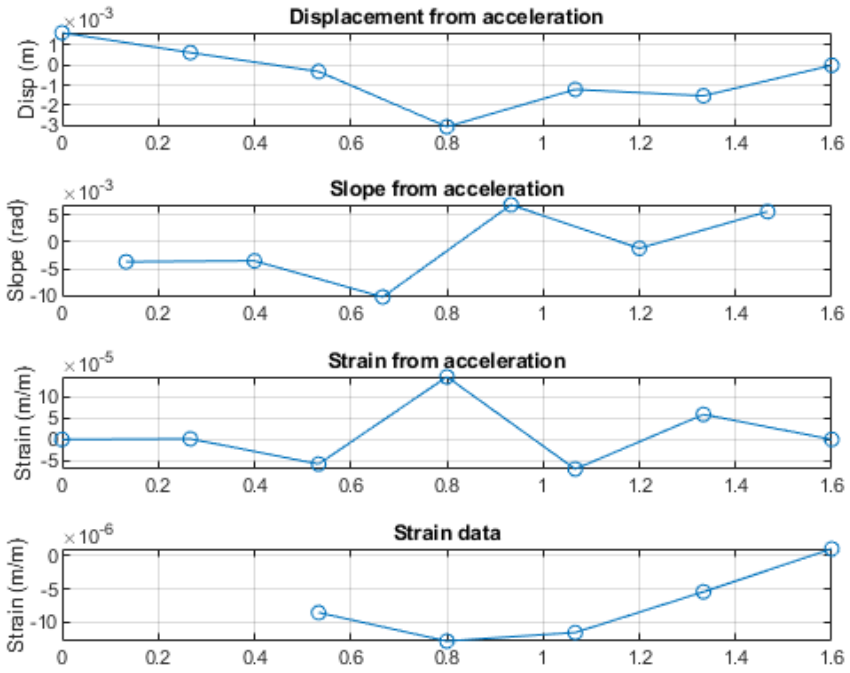

Figure 27: Low frequency experimental displacement to strain transform results from accelerometer data, with poor symmetry in displacement due to unmatched accelerometer sensitivities

In hindsight, this could easily have been verified at the start of the experiments by mounting two or more accelerometers next to each other, declaring the accelerometer with the most recent calibration certificate to be the baseline and comparing the measurements obtained. The sensitivity could then have been adjusted in the channel setup to yield the same results as the baseline accelerometer. This adjustment would be temporary since the sensitivity needs to be declared in the channel setup for each accelerometer. This form of rough calibration would have resulted in smoother acceleration curves for the beam with measurements that have realistic amplitudes relative to other measuring points on the beam.

The small displacements in this test case did not cause significant strain in the beam and as a result, the strain amplitudes were close to the strain gauge noise floor. This caused relatively high levels of noise to be present in the strain measurements of this test case. These noise components would also be present in the rainflow cycle counts after the data was processed with a notch comb filter. In hindsight, considering the low natural frequencies of the beam and the high frequency components generated in the beam through modal hammer impacts, it would have been better to set the sample rate to a lower frequency of 1000 Hz. Even with the noise included in the cycle counts, this test case resulted in zero accumulated damage from both the traditional strain measurements and the transformed acceleration measurements.

If the aim was to obtain clear cycle counts for the strain gauge measurements, a low pass filter could be employed to remove all frequencies from 48 Hz and up to remove all noise from the local electrical grid frequency.

4.4.2 Combined low and high frequency results

During the combined low and high frequency experiment, large displacements were prioritised. The beam was allowed to be slightly out of phase with the shaker, while ensuring that the shaker signal amplifier's overload warning light did not indicate that the signal voltage is too high. While setting the shaker's displacement amplitude, the author monitored the sound made by the shaker to ensure that the shaker did not start to make contact with its casing at the limits of its displacement range.

An example of the strain and acceleration measurements with the combined low and high frequency components at the time of an impact, is shown in Figure 28.

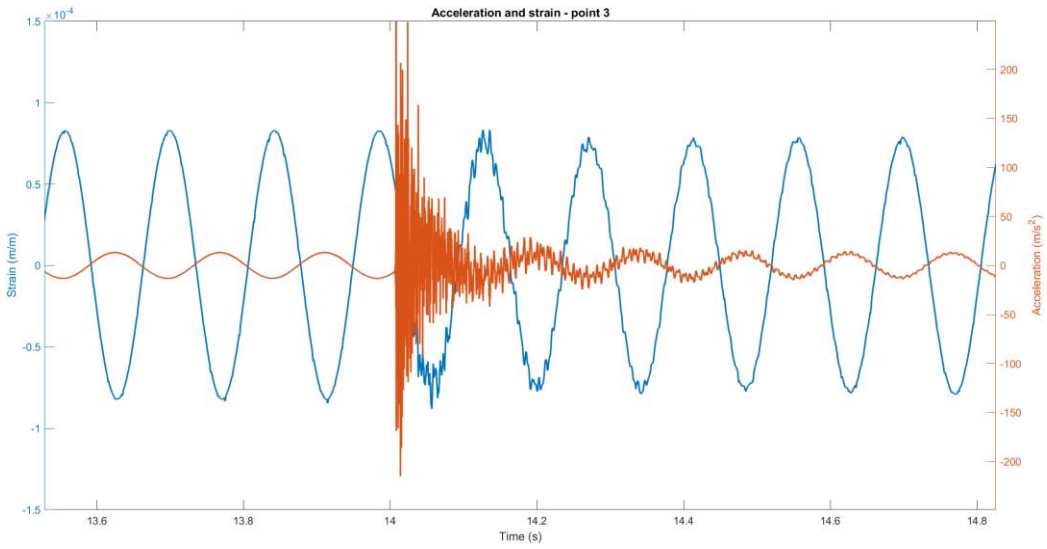

Figure 28: Cyclic loading with low and high frequency components

The modal hammer impacts excited the beam at its natural frequencies, as is shown in the fast Fourier transform (FFT) diagrams in Figure 29 for Measuring Point 4.

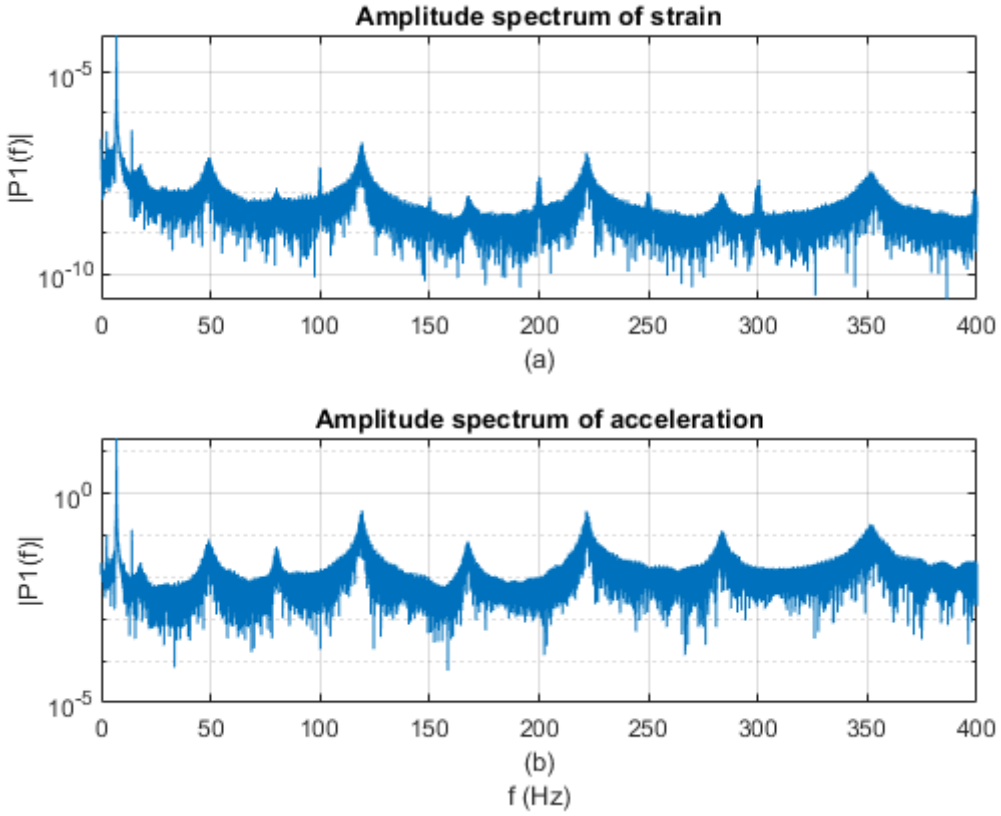

Figure 29: Combined low and high frequency strain (a) and acceleration (b) FFT of test specimen at Point 4

A sharp peak is shown at the 7 Hz frequency, by gradual peaks at each natural frequency starting with the first five natural frequencies in Table 2. Figure 33 (a) also shows the 50 Hz electrical noise and its harmonics as mentioned previously. Peaks at 3 Hz and 18 Hz can also be seen, but their cause is unknown.

The time domain acceleration response of this test case, as well as the transformed velocity and displacement is shown in Figure 30 below. There are sharp increases in acceleration as the beam is impacted, but the effect on displacement is relatively small. It would be possible to separate the low and high frequency components of the vibration by simply applying a low pass filter to obtain the low frequency components and a high pass filter to obtain the high frequency component. Rainflow load cycle counts can then be conducted on the separate frequency responses to finally obtain the damage contributed by each frequency component.

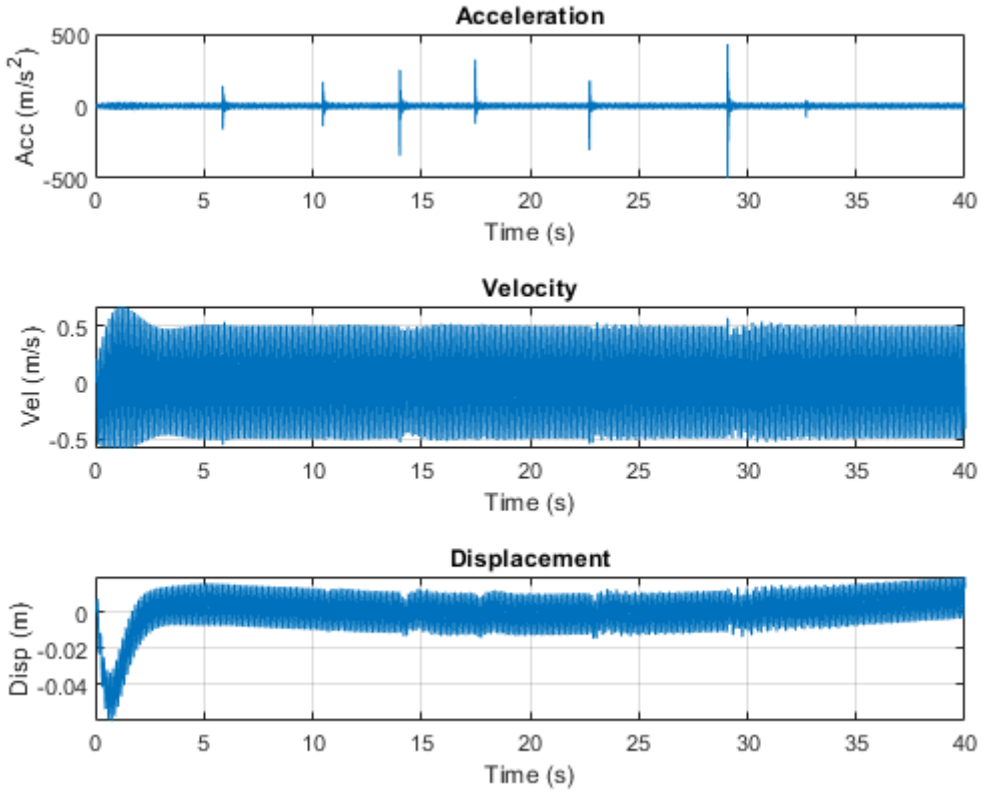

Figure 30: Combined low and high frequency acceleration to displacement transform results

The results of the displacement to strain transform were similar to that of the previous low frequency test run shown in Figure 27 and discussed in Section 4.4.1. The transformed strains obtained from acceleration was, however, much larger than the measured strain gauge strain. The maximum transformed stress from the acceleration's amplitude is found to be 464.39 MPa, which is far larger than the stress amplitude from the measured strain at 22.81 MPa.

The rainflow stress cycle counting for the transformed acceleration stresses displayed in Figure 31 in Pa indicates that for the majority of the time range the stress cycles oscillated around zero and that a few cycles were larger than the bulk as can be expected due to the modal hammer impacts. This method proved to be unreliable for determining the stresses in the structure since it gave values much larger than those in the verification strain measurement data set.

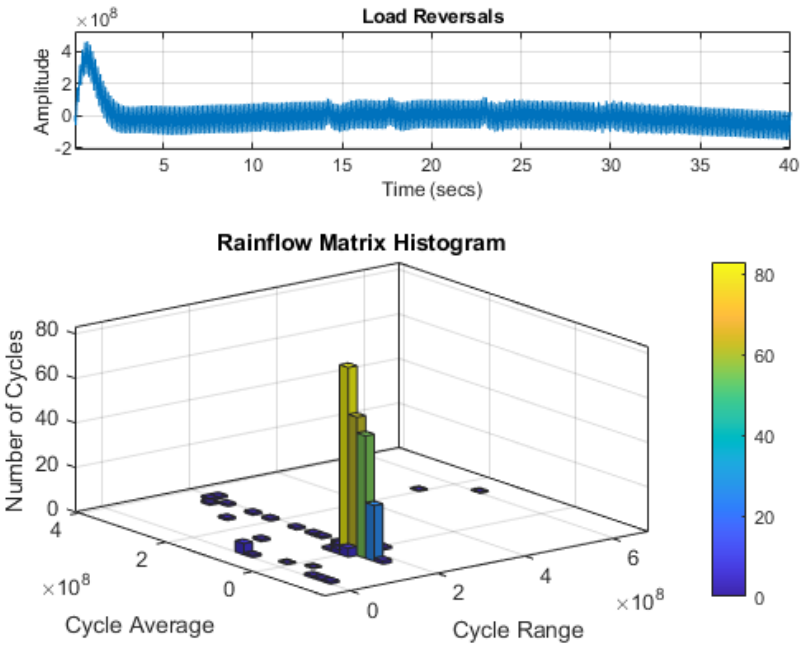

Figure 31: Combined low and high frequency acceleration stress rainflow count in Pa

The stress rainflow counting for the strain stress measurements indicates that the majority of the load cycles had a stress range of 37 MPa with some variation around that point, due to the modal hammer impacts. There is also high frequency noise with a cycle average of ±2 MPa. This was visible in the time domain strain data at the peaks of the strain measurements, where the gradient of the strain became zero, causing the measurement to be steady for a moment and the noise floor to become more visible in the measurements. This could be mitigated by setting the sample rate to a lower frequency and increasing the bridge excitation voltage (Figliola & Beasley, 2019).

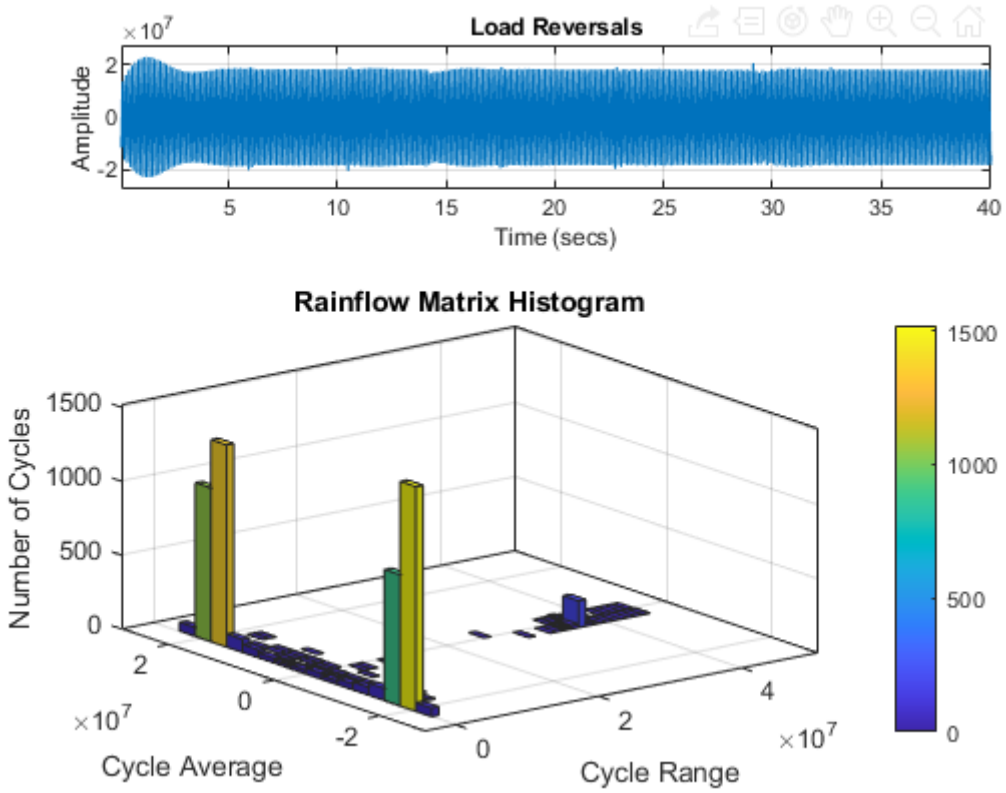

Figure 32: Combined low and high frequency strain stress rainflow count

Even at the extremities of the experimental rig capabilities, the resulting accumulated damage was still 0 for the strain stress measurements. The transformed stress measurement data set shown, did however have two anomalies that caused a total damage number of 0.5 to be obtained. Considering the displacements achieved and loads applied to the beam, this is an unreasonable result and it is safe to say that these anomalous values are not accurate measurements.

Further refinement of this method could result in it being viable for obtaining stress measurements from accelerometer networks on a known structure such as a beam. Suggested changes would be to use a lower sampling frequency to reduce measured noise and to increase the number of accelerometers and verify their calibration. Another refinement that is required is improvement of the filtering step of the algorithm to completely remove high frequency noise. Another possible way in which the noise can be mitigated is by increasing the excitation voltage over the bridge (Figliola & Beasley, 2019).

5 Conclusions

This project had the overarching goal of investigating an alternative method for obtaining accumulated fatigue damage from accelerometer measurements instead of traditional strain gauge measurements for structures in operation experiencing cyclic loads. To achieve this goal, an intermediate objective was required for obtaining the location of maximum strain in the structure to monitor for fatigue damage.

Considering the results obtained from the EMA, the first objective of investigating a method for transforming displacement mode shapes to strain mode shapes can be considered a success since the second objective was achieved. It verified the results obtained from both the theoretical method and numeric data transformation methods.

The second half of the project, namely the final overarching goal of obtaining an accumulated damage number using an alternative method with accelerometer measurements instead of traditional strain gauge measurements, was not a complete success. The alternative method proved to be inaccurate, yielding results that were far larger than the verification strain measurements. The second half of the project, discussed in Chapter 4, did however result in the writing of an algorithm that can be used to obtain the accumulated damage from a strain data set. Further refinements of both the alternative method and the experimental rig are suggested in order to be certain that the alternative method of determining accumulated fatigue damage is not viable for a known beam structure.

The experimental method employed in this project can be improved in several ways. This experimental rig required numerous strain gauge bridges, although the theoretical modal analysis results can be verified using only one strain gauge bridge and accelerometer pair and a roving impact with a modal hammer. Depending on the excitation frequencies experienced by the structure during operation, there could be one location of maximum strain or multiple locations of high strain. By first determining and verifying these locations to be monitored, less strain gauges can be utilised, resulting in the saving of time, cost and resources (see Appendix F), as is the motivations for objectives one and two. The need for of multiple accelerometers for the cyclic loading experiments does remain and this project has shown the importance of proper calibration and time synchronisation when utilising an accelerometer network for such an experiment. The need for a full strain gauge bridge for experiments of this nature is debatable, but it did demonstrate that even when employing common mode rejection, external noise sources can still be a problem.

Suggested improvements of the experimental rig that was constructed include changes in the wiring of the test rig to reduce noise. This can be done by procuring shielded cables with the required connectors for the full length of the strain gauge bridge connections to the DAS and creating twisted pairs in the bridge connection wires. Replacing the IMV Vibro PET-01 shaker with a shaker with a larger displacement capability is also suggested. Finally, the test specimen can be altered by introducing one or multiple stress concentrations to the beam by simply decreasing the cross-sectional area at one or more of the measuring points. If this changed experimental rig still does not result in loads that cause accumulated fatigue damage, the author would suggest constructing an alternative rig that utilize a fatigue loading machine with high load hydraulic actuators.

For future research on this topic at Stellenbosch University, a rig can utilize the MSI fatigue loader available at the structures laboratory of the Mechanical and Mechatronic Department. With the use of a fatigue testing machine, a completely different experimental setup can be devised that also tests to failure and verifies the fatigue life estimate. Such an experimental setup would however require multiple test samples to be tested to failure since SN curves are generated using multiple data points and the estimated cycles to failure at a specific stress range is an average.

Considering the methods tested and results obtained in this project, it is viable to make use of accelerometer networks to obtain the location of maximum strain in a marine vessel, but the author does not suggest making use of those accelerometer networks to conduct fatigue analysis to obtain a structural accumulated fatigue damage estimate. Considering the scale and complexity of a marine vessel compared to a beam, the time synchronisation of measurements would be essential to ensure that measurements do not indicate that one part of the ship is in an inaccurate position relative to another one. Depending on the size of the vessel, millimetres or centimetres of inaccuracy in displacement calculations from accelerometer data would make it impossible to determine if highly damaging cyclic loads occurred. By making use of appropriate strain gauges, shielded cables and high excitation voltages, while taking care to minimise noise in the measurement system, a traditional strain gauge network would be the appropriate sensor network for a hull monitoring system.

6 References

American Society for Testing and Materials. 2011. ASTM Designation E1049-85 R11: Standard Practice for Cycle Counting in Fatigue Analysis. ASTM International. In: ASTM standards on disc standards worldwide. *Section three, Metals test methods and analytical procedures*. 2012. West Conshohocken: ASTM International.

Avitabile, P. 2018. *Modal Testing: A Practitioner's Guide.* Hoboken, New Jersey: Wiley.

Bai, Y. & Jin, W.L. 2016. *Marine Structural Design*. 2nd Ed. Oxford: Elsevier.

Budynas, R.G. & Nisbett, J.K. 2015. *Shigley's Mechanical Engineering Design*. 10th Ed. New York: McGraw-Hill.

Caresta, M., 2016. *Vibrations of a Free-Free Beam.* http://www.varg.unsw.edu.au/Assets/link%20pdfs/Beam_vibration.pdf [2022, July 13].

Dowling, N.E., Kampe, S.L. & Kral, M.V. 2019. *Mechanical Behaviour of Materials: Engineering Methods for Deformation, Fracture and Fatigue.* 5th Ed. Harlow: Pearson Education.

Ewins, D.J. 2000. *Modal Testing: Theory, Practice and Application*. 2nd Ed. Bognor Regis: John Wiley & Sons Ltd.

Figliola, R.S. & Beasley, D.E. 2019. *Theory and design for mechanical measurements.* 7th Ed. Hoboken: John Wiley & Sons.

HBM. [s.a.]. *LY Linear Strain Gauges with 1 Measuring Grid* [Electronic]. Available: https://www.hbm.com/en/4561/ly-linear-strain-gauges-with-1-measurement-grid/?product_type_no=LY%20Linear%20Strain%20Gauges%20with%201%20Measuring%20Grid [2022, October 16].

Hibbeler, R.C. 2017. *Engineering Mechanics Dynamics.* 14th Ed. Harlow: Pearson Education.

IMV. [s.a.]. *Product Specifications – IMV Corporation*. https://www.imv-global.com/specifications/?lang=en&id=01&type=small&s=pet#iframe-sheet [2022, October 16].

Inman, D.J. 2014. *Engineering Vibration*. 4th Ed. Essex: Pearson Education Ltd.

Li, Z. 2011. *Direct Calculation of Wave-Induced Loads and Fatigue Damage of Container Vessels*, Gothenburg: Chalmers Reproservice.

MathWorks. [s.a.]. *rainflow – Rainflow counts for fatigue analysis* [Online]. Available: https://www.mathworks.com/help/signal/ref/rainflow.html [2022, October 19].

PCB Piezotronics. [s.a.] a. *Model: 333B32 | Accelerometer, ICP* [Online]. Available at: https://www.pcb.com/products?model=333B32 [2022, July 3].

PCB Piezotronics. [s.a.] b. *Model: 208C03 | ICP Force Sensor* [Online]. Available: https://www.pcb.com/products?m=208C03 [2022, October 16].

PCB Piezotronics. [s.a.] c. *Model: 086C01 | Impact Hammer, ICP* [Online]. Available: https://www.pcb.com/products?m=086C01 [2022, July 3].

Siemens. 2019. *How to measure strain gauges with Simcenter Testlab?* [Electronic]. Available: https://community.sw.siemens.com/s/article/how-to-measure-strain-gauges-with-simcenter-testlab [2022, October 15].

Siemens. 2022. *Simcenter SCADAS Mobile and SCADAS Recorder* [Online]. https://community.sw.siemens.com/s/article/simcenter-scadas-mobile-and-scadas-recorder [2022, October 16].

Sorber, E. [s.a.]. Modal Seminar Series: Modal Analysis Introduction – Basics of Vibration, Sensors & Instrumentation. [Online] Available at: https://www.plm.automation.siemens.com/global/en/webinar/modal-analysis-onlinemasterclass-session2/97056 [2022, March 29].

Transducer Techniques, 2022. https://www.transducertechniques.com/wheatstone-bridge.aspx [2022, August 19].

Appendix A Sample calculations

See https://github.com/Christo-JvV/Fatigue-Analysis for full MATLAB algorithm.

A.1 Test sample modal analysis

```
% ~~~~~~~~~~~~~~~~~~~~~~~~~~~~~~~~~~~~~~~~~~~~~~~~~~~~
% # Experimental modal analysis (EMA) disp and strain
% ~~~~~~~~~~~~~~~~~~~~~~~~~~~~~~~~~~~~~~~~~~~~~~~~~~~~
% Author: HC Janse van Vuuren
% Date: 25/09/2022
% ~~~~~~~~~~~~~~~~~~~~~~~~~~~~~~~~~~~~~~~~~~~~~~~~~~~~
clear


% # Flat bar Modal analysis
% Parameters
Length = 1.6;       %m
b = 40;             %mm
t = 4.5;            %mm
A_mm = b*t;         %mm^2
A = A_mm*1000^-2;   %m^3
I_mm = b*(t^3)/12;  %mm^4
I = I_mm*1000^-4    %m^4
```

```
I = 3.0375e-10
```

```
rho = 7800;         %kg/m^3
E = 200*10^9;       %Pa
m = A*Length*rho    %kg
```

```
m = 2.2464
```

```
BetaL = [4.73004074 7.85320462 10.9956078 14.1371655 17.2787597];
Beta = BetaL/Length;

wn = (Beta.^2)*sqrt((E*I)/(rho*A));  %rad/s
fn = wn/(2*pi)      %Hz
```

```
fn = 1×5
    9.1495   25.2211   49.4434   81.7324  122.0942
```

```
% # Free-free beam mode shapes
L = 1;
BL = [4.73004074 7.85320462 10.9956078 14.1371655 17.2787597]';
B = BL/L;
x = linspace(0,L);


% Measuring points
measuring = 7;
points = linspace(0,L,measuring);
```

```
ypoints = zeros(1,measuring);


sigma = ( cosh(B*L) - cos(B*L) ) ./ ( sinh(B*L) - sin(B*L) );
c_sigma = 1./(-1.*sigma);


% Displacement mode shapes
vx =  sinh(B.*x) + sin(B.*x) + c_sigma.*(cosh(B.*x) + cos(B.*x));
X = sinh(B.*x) + sin(B.*x) + (sin(BL)-sinh(BL)) ./ (cosh(BL)-
cos(BL)) .* (cosh(B.*x)+cos(B.*x));


% Normalise displacement mode shapes to unity
for i = 1:5
    X(i,:) = X(i,:) / max( abs(X(i,:)) );
end


% Distance from beam mid-line to surface
yy = t/1000;    %(m)
z = yy/2;       %(m)


% Second derivative of displacement
M_EI = ( sinh(B.*x) - sin(B.*x) + c_sigma.*(cosh(B.*x) - cos(B.*x))
).*(B.^2);  % Moment shapes divided by EI
eX = M_EI*(z);  %strain mode shapes


% Normalise strain mode shapes to unity
for i = 1:5
    eX(i,:) = eX(i,:) / max( abs(eX(i,:)) );
end


% Plot all displacement mode shapes
plot(x,X(1, 1:end), x,X(2, 1:end), x,X(3, 1:end), x,X(4, 1:end),
x,X(5, 1:end))
hold on
plot(points,ypoints,'*r')
grid on
title('First 5 displacement mode shapes of a free-free beam.')
legend('1st Mode','2nd Mode','3rd Mode', '4th Mode', '5th Mode')
xlabel('Normalised Length (x/L)')
hold off
```

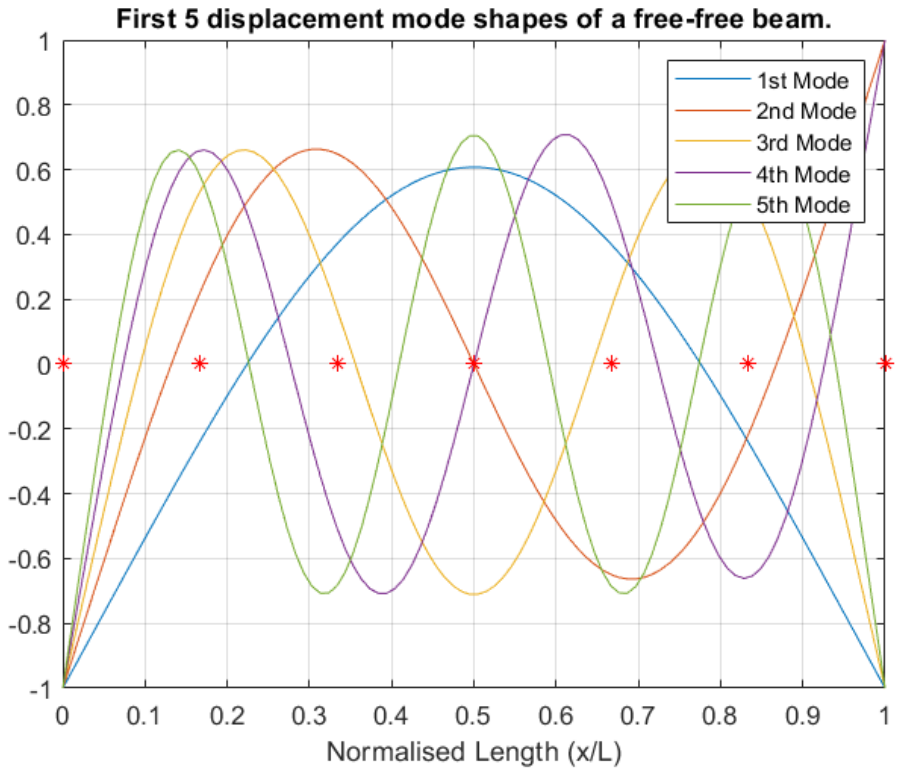

Figure 33: First five displacement mode shapes with measuring points

```
% Plot all strain mode shapes
plot(x,eX)
hold on
plot(points,ypoints,'*r')
grid on
title('First 5 strain mode shapes of a free-free beam.')
legend('1st Mode','2nd Mode','3rd Mode', '4th Mode', '5th Mode')
xlabel('Normalised Length (x/L)')
hold off
```

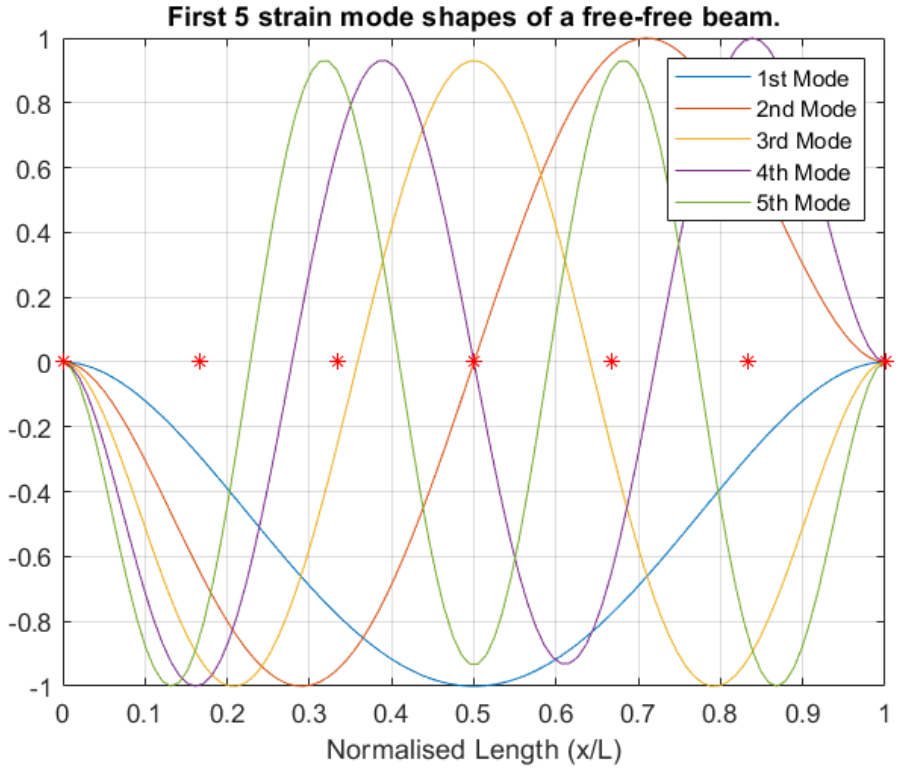

Figure 34: First five strain mode shapes with measuring points

A.2 Fatigue damage calculations

```
% ##############################
% ~~~~~~~~~~~~~~~~~~~~~~~~~~~~~~
% Calculate damage number from acceleration
% and strain data and compare them.
% ~~~~~~~~~~~~~~~~~~~~~~~~~~~~~~
% Author: HC Janse van Vuuren
% Date: 11/10/2022
% ~~~~~~~~~~~~~~~~~~~~~~~~~~~~~~
% ##############################
clear
% ~~~~~~~~~~~~~~~~~~~~~~~~~~~~~~
%% # Beam and material properties
% ~~~~~~~~~~~~~~~~~~~~~~~~~~~~~~
% Beam Parameters
Length = 1.6;       % Beam lenth (m)
width = 40/1000;    % Beam width (m)
th = 4.5/1000;      % Beam thickness (m)
A = width*th;       % Beam cross sectional area (m^3)
I = width*(th^3)/12;% Beam moment of inertia about the z-axis (m^4)
rho = 7800;         % Beam mild steel density (kg/m^3)
```

```
E = 200*10^9;       % Beam mild steel Young's modulus (Pa)
m = A*Length*rho;   % Beam mass (kg)


% S-N curve for commercial grade mild steel
% 1045 Plain carbon (mild) steel HR,N - SN curve (Shigley)


S = [80 70 56 47 47 47 47].*6894.757./1000;     % Stress range to
failure (MPa)
N = [1e4 4e4 1e5 4e5 1e6 4e6 1e7];      % Cycles to failure


ST = 107.*6894.757./1000;   % Tensile strength (MPa)
SY = 63.*6894.757./1000;    % Yield strength (MPa)


b1 = ( log(S(1)/S(2)) / log(N(1)/N(2)) );   % SN curve exponent
constant b
b2 = ( log(S(2)/S(3)) / log(N(2)/N(3)) );   % SN curve exponent
constant b
b3 = ( log(S(3)/S(4)) / log(N(3)/N(4)) );   % SN curve exponent
constant b
a1 = S(1)/(N(1)^b1);   % SN curve scaling constant a
a2 = S(2)/(N(2)^b2);   % SN curve scaling constant a
a3 = S(3)/(N(3)^b3);   % SN curve scaling constant a
a4 = S(end);           % SN curve scaling constant a


N1 = @(s) (s/a1)^(1/b1);    % N-S curve (Cycles-MPa) for 551.58056 >
s >= 482.63299
N2 = @(s) (s/a2)^(1/b2);    % N-S curve (Cycles-MPa) for 482.63299
      > s >= 386.106392
N3 = @(s) (s/a3)^(1/b3);    % N-S curve (Cycles-MPa) for 386.106392
> s >= 324.053579
N4 = @(s) s-s + inf;        % N-S curve (Cycles-MPa) for 324.053579
> s


% Generate SN curve values
s = linspace(S(4),S(1));    % SN curve stress range
n = zeros(length(s),1);     % SN curve cycle range


for i = 1:length(n)
    if S(1) <= s(i)
        n(i) = 1;
    elseif S(1) > s(i) && s(i) >= S(2)
        n(i) = N1(s(i));
    elseif S(2) > s(i) && s(i) >= S(3)
```

```
        n(i) = N2(s(i));
    elseif S(3) > s(i) && s(i) >= S(4)
        n(i) = N3(s(i));
    elseif S(4) > s(i)
        n(i) = inf;
    end
end
% Plot SN curve
```

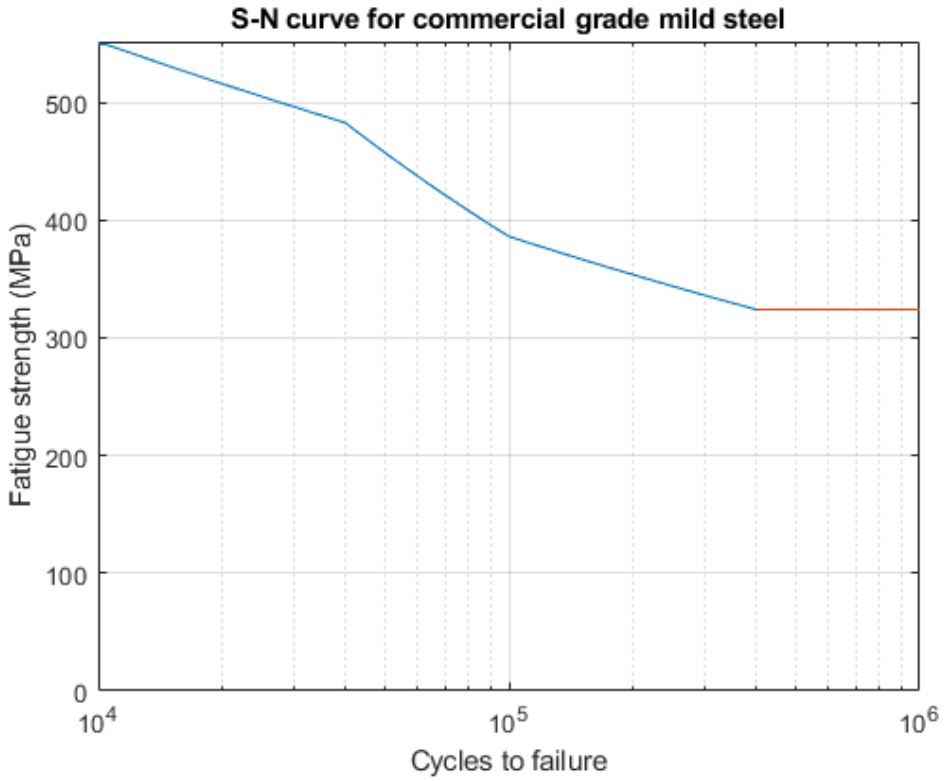

Figure 35: 1045 Plain carbon steel piecewise SN curve

```
% ~~~~~~~~~~~~~~~~~~~~~~~~~~~~~~~
%% # Sensor data import
% ~~~~~~~~~~~~~~~~~~~~~~~~~~~~~~~
Run18T = importdata('Run 18 Throughput.mat');% Import all
measurement data of run
dt = Run18T.Signal_0.x_values.increment;     % Sampling period -
Length of each time step (s)
fs =  1/dt;                                  % Sampling frequency
(Hz)
tend = Run18T.Signal_0.x_values.start_value +
(Run18T.Signal_0.x_values.number_of_values-1) * dt;
t = Run18T.Signal_0.x_values.start_value : dt : (tend); % Time range
entries = length(t);                                    % Data array
length
```

```
acc = Run18T.Signal_2.y_values.values(1:entries,:);     % Whole
acceleration data set (m/s^2)
strainData = Run18T.Signal_0.y_values.values;     % Whole strain
data set (m/m)
stress = strainData.*E;     % Whole strain data set (m/s^2)


measPointsA = min(size(Run18T.Signal_2.y_values.values));
%number of acceleration measuring points
measPointsS = min(size(Run18T.Signal_0.y_values.values));
%number of strain measuring points


x = linspace(0,Length,measPointsA);     % Position range along the
x-axis (beam length) (m)
dx = x(2) - x(1);                       % Distance between
measutring points (m)
% ~~~~~~~~~~~~~~~~~~~~~~~~~~~~~~~
% Acc to disp (integrate in time)
% ~~~~~~~~~~~~~~~~~~~~~~~~~~~~~~~
% Declare variables
accD = zeros(size(acc));    % Detrended acceleration (m/s^2)
acc2 = zeros(size(acc));    % Filtered acceleration (m/s^2)
vel = zeros(size(acc));     % Velocity (m)
disp = zeros(size(acc));    % Displacement (m)


% Acceleration data sets are integrated twice to determine
displacement
for i = 1:measPointsA

    accD(1:entries, i) = detrend(acc(1:entries, i));

    % Highpass filter at '0' Hz
    N = 2;    % Filter order
    fc = 0.5; % Cut off frequency (Hz)
    [B1,A1] = butter(N,2*fc/fs,'high'); % Butterworth filter
constants
    acc2(1:entries, i) = filter(B1,A1,accD(1:entries, i));

    % Velocity
    vel(1:entries, i) = cumtrapz(dt,acc2(1:entries, i));
    vel(1:entries, i) = detrend(vel(1:entries, i));

    % Displacement
    disp(1:entries, i) = cumtrapz(dt,vel(1:entries, i));
end
```

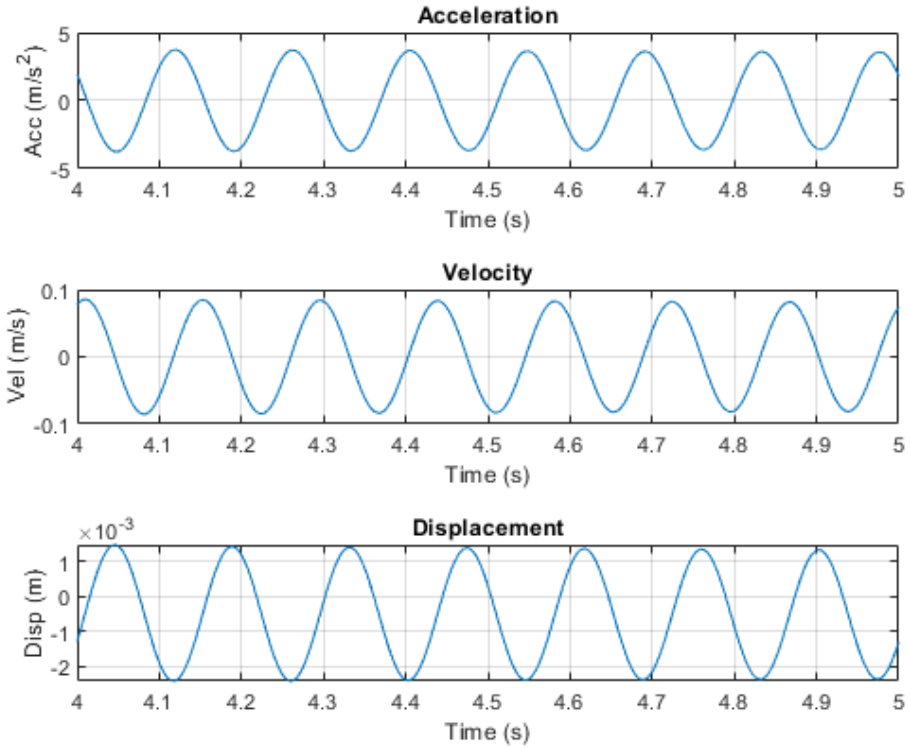

Figure 36: Low frequency run integration results

```
% ~~~~~~~~~~~~~~~~~~~~~~~~~~~~~~~
% Disp to Stress (differentiate in position and convert)
% ~~~~~~~~~~~~~~~~~~~~~~~~~~~~~~~
% Distance from beam mid-line to surface
z = th/2;      %(m)


% Declare
slope  = zeros(length(disp),(measPointsA-1)); %slope obtained from
acc
strainA_z = zeros(size(disp));  %strain obtained from acc over z


% Differentiate with two point difference due to low spatial
resolution
for i = 1:entries
    slope(i,1:6) = (diff(disp(i,:)))./dx;
    strainA_z(i,2:6) = (diff(slope(i,:)))./dx;
end


% Convert to strain and stress
strainA = strainA_z.*z;         %strain obtained from acc
```

```
stressA = strainA_z.*z.*E;      %stress obtained from acc


% Plot differentiation steps
```

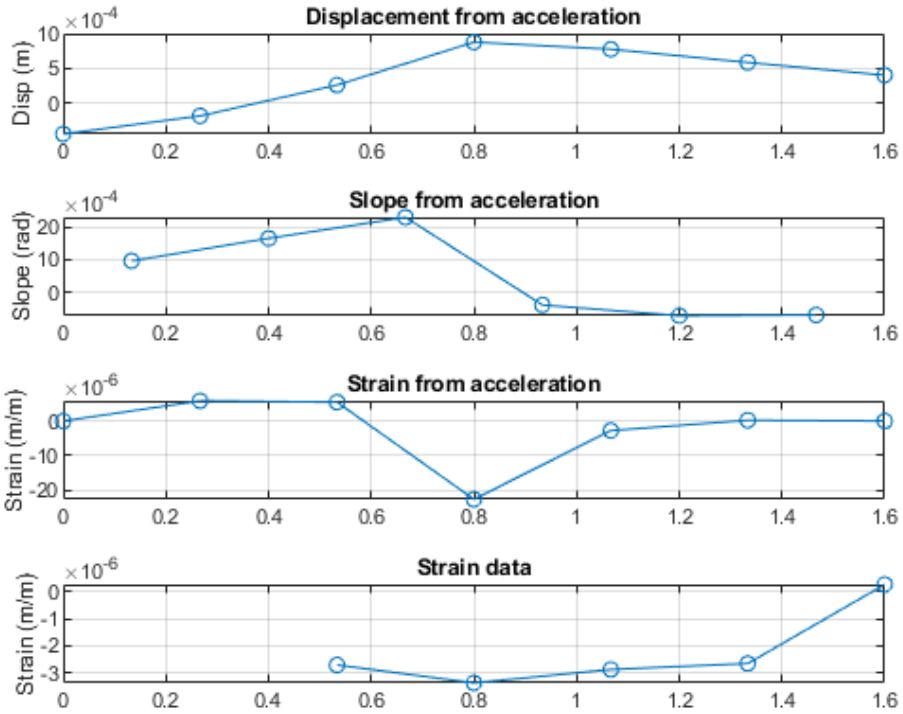


```
% ~~~~~~~~~~~~~~~~~~~~~~~~~~~~~~~
% Rainflow counting - Acc stress
% ~~~~~~~~~~~~~~~~~~~~~~~~~~~~~~~


% Find measuring point with max stress
[MaxStressesA, MaxIndiciesA] = max(abs(stressA));
[MaxStressA, MaxStressLocationA] = max(MaxStressesA);
stressA4 = stressA(1:entries, MaxStressLocationA);
maxk(abs(stressA4),5)
```

```
ans = 5×1
10^8 ×
    4.6439
    4.6439
    4.6438
    4.6438
    4.6437
```

```
% Conduct rainflow count to obtain stress ranges and cycle counts
% Acceleration stress rainflow count plots:
rainflow(stressA4,t)
```

See Figure 31: Combined low and high frequency acceleration stress rainflow count in Pa.

```
% Acceleration stress rainflow count data
[cA,histA,edgesA,rmmA,idxA] = rainflow(stressA4,t);


StressAccRainflowTable =
array2table(cA,'VariableNames',{'Count','Range','Mean','Start','End'
});
histogram('BinEdges',edgesA','BinCounts',sum(histA,2))
title('Acc stress cycle counts')
xlabel('Acc stress range (Pa)')
ylabel('Cycle counts')
```

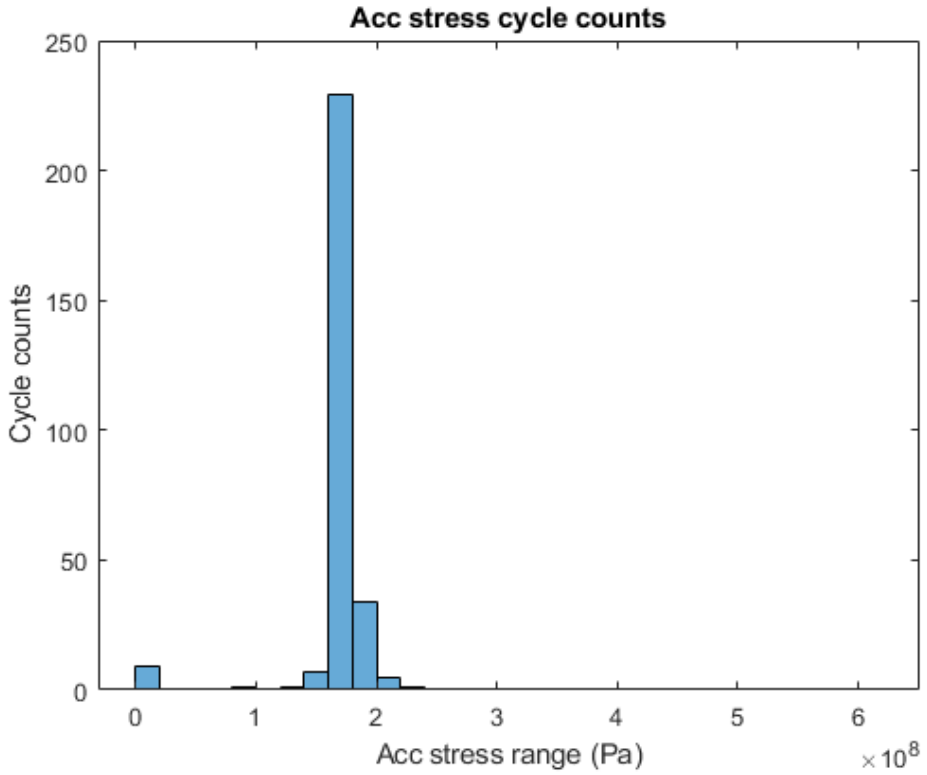


```
% ~~~~~~~~~~~~~~~~~~~~~~~~~~~~~~~
% Damage number -  Acc stress
% ~~~~~~~~~~~~~~~~~~~~~~~~~~~~~~~
% Assign and declare vatiables
StressAccRanges = StressAccRainflowTable{:,'Range'}/1e6;  %
Accelearation stress range (MPa)
StressAccCounts = StressAccRainflowTable{:,'Count'};  %Accelearation
stress cycle counts
StressAccLives = zeros(length(StressAccRanges),1); %Number of cycles
to failure at acceleration stress range
```

```
% Find acceleration stress life estimates
for i = 1:length(StressAccLives)
    if S(1) <= StressAccRanges(i)
        StressAccLives(i) = 1;
    elseif S(1) > StressAccRanges(i) && StressAccRanges(i) >= S(2)
        StressAccLives(i) = N1(StressAccRanges(i));
    elseif S(2) > StressAccRanges(i) && StressAccRanges(i) >= S(3)
        StressAccLives(i) = N2(StressAccRanges(i));
    elseif S(3) > StressAccRanges(i) && StressAccRanges(i) >= S(4)
        StressAccLives(i) = N3(StressAccRanges(i));
    elseif S(4) > StressAccRanges(i)
        StressAccLives(i) = inf;
    end
end


%Calculate damage of individual cyces
dd_StressAccDamages = StressAccCounts./StressAccLives;
% Calculate total damage of test run from acceleration
D_StressAccDamage = sum(dd_StressAccDamages)
```

```
D_StressAccDamage = 0.5000
```

```
% ~~~~~~~~~~~~~~~~~~~~~~~~~~~~~~~
% Rainflow counting - Strain stress
% ~~~~~~~~~~~~~~~~~~~~~~~~~~~~~~~
% Find measuring point with max stress
[MaxStresses, MaxIndicies] = max(abs(stress));
[MaxStress, MaxStressLocation] = max(MaxStresses);
stress4 = stress(1:entries, MaxStressLocation);
maxk(abs(stress4),5)
```

```
ans = 5×1
10^7 ×
    2.2810
    2.2810
    2.2808
    2.2805
    2.2805
```

```
% Filter data
% Highpass filter at '0' Hz
N = 3;  % filter order
fc = 0.5; % cut off frequency (Hz)
[B,A] = butter(N,2*fc/fs,'high');


stress4filtered = filter(B,A,stress4);


% Band stop (notch) comb filter for 50 Hz and its products
```

```
v = 8;              %number of notch filters
a = zeros(1,v);
aa = zeros(1,v);


for i = 1:v
    a(i) = i*50 - 1;
    aa(i) = i*50 + 1.5;

    bsFilt(i) = designfilt('bandstopiir','FilterOrder',20, ...
         'HalfPowerFrequency1',a(i), ...
         'HalfPowerFrequency2',aa(i),...
         'SampleRate',fs);

    stress4filtered = filter(bsFilt(i),stress4filtered);
end


% Conduct rainflow count to obtain stress ranges and cycle counts
rainflow(stress4filtered,t)
```

See Figure 32: Combined low and high frequency strain stress rainflow count in Pa.

```
[c,hist,edges,rmm,idx] = rainflow(stress4filtered,t);


StressRainflowTable =
array2table(c,'VariableNames',{'Count','Range','Mean','Start','End'}
);
histogram('BinEdges',edges','BinCounts',sum(hist,2))
title('Strain stress cycle counts')
xlabel('Stress Range')
ylabel('Cycle Counts')
```

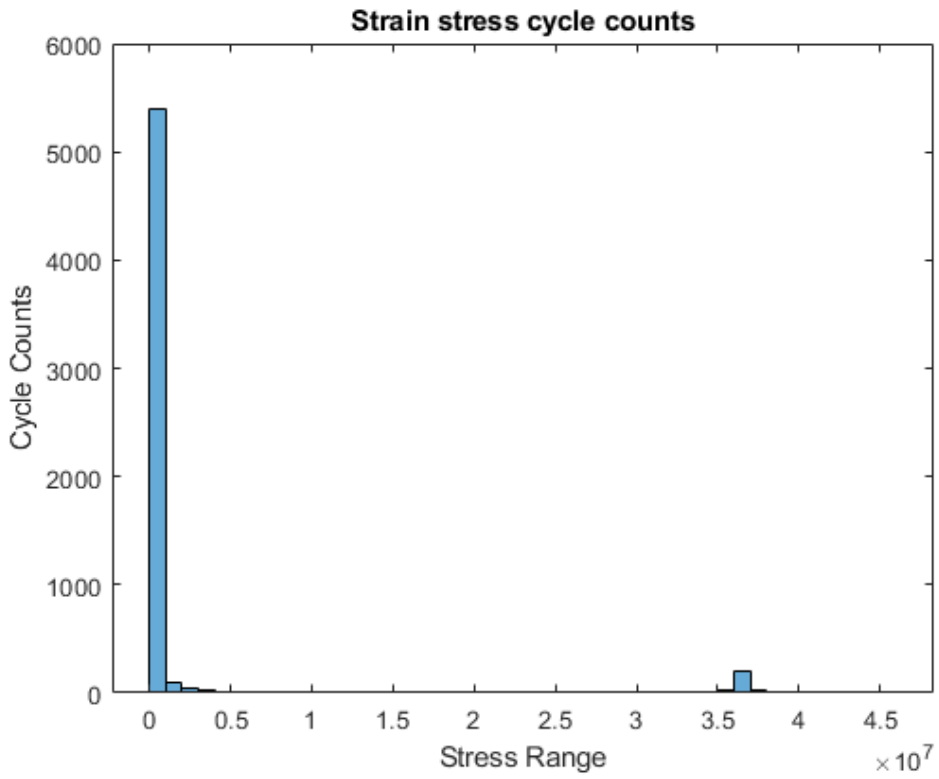


```
% ~~~~~~~~~~~~~~~~~~~~~~~~~~~~~~~
% Damage number - Strain stress
% ~~~~~~~~~~~~~~~~~~~~~~~~~~~~~~~


% Assign and declare vatiables
StressRanges = StressRainflowTable{:,'Range'}/1e6;  % Stress range
(MPa)
StressCounts = StressRainflowTable{:,'Count'};  % Stress cycle
counts
StressLives = zeros(length(StressRanges),1); % Number of cycles to
failure at stress range


% Find stress life estimates
for i = 1:length(StressLives)
    if S(1) <= StressRanges(i)
        StressLives(i) = 1;
    elseif S(1) > StressRanges(i) && StressRanges(i) >= S(2)
        StressLives(i) = N1(StressRanges(i));
    elseif S(2) > StressRanges(i) && StressRanges(i) >= S(3)
        StressLives(i) = N2(StressRanges(i));
    elseif S(3) > StressRanges(i) && StressRanges(i) >= S(4)
        StressLives(i) = N3(StressRanges(i));
    elseif S(4) > StressRanges(i)
        StressLives(i) = inf;
```

```
    end
end


%Calculate damage of individual cyces
dd_StressDamages = StressCounts./StressLives;
% Calculate total damage of test run from strain
D_StressDamage = sum(dd_StressDamages)
```

```
D_StressDamage = 0
```

```
% ~~~~~~~~~~~~~~~~~~~~~~~~~~~~~~~
% Tabulate and compare results
% ~~~~~~~~~~~~~~~~~~~~~~~~~~~~~~~
D_StressAccDamage
```

```
D_StressAccDamage = 0.5000
```

```
D_StressDamage
```

```
D_StressDamage = 0
```

Appendix B Test sample drawing

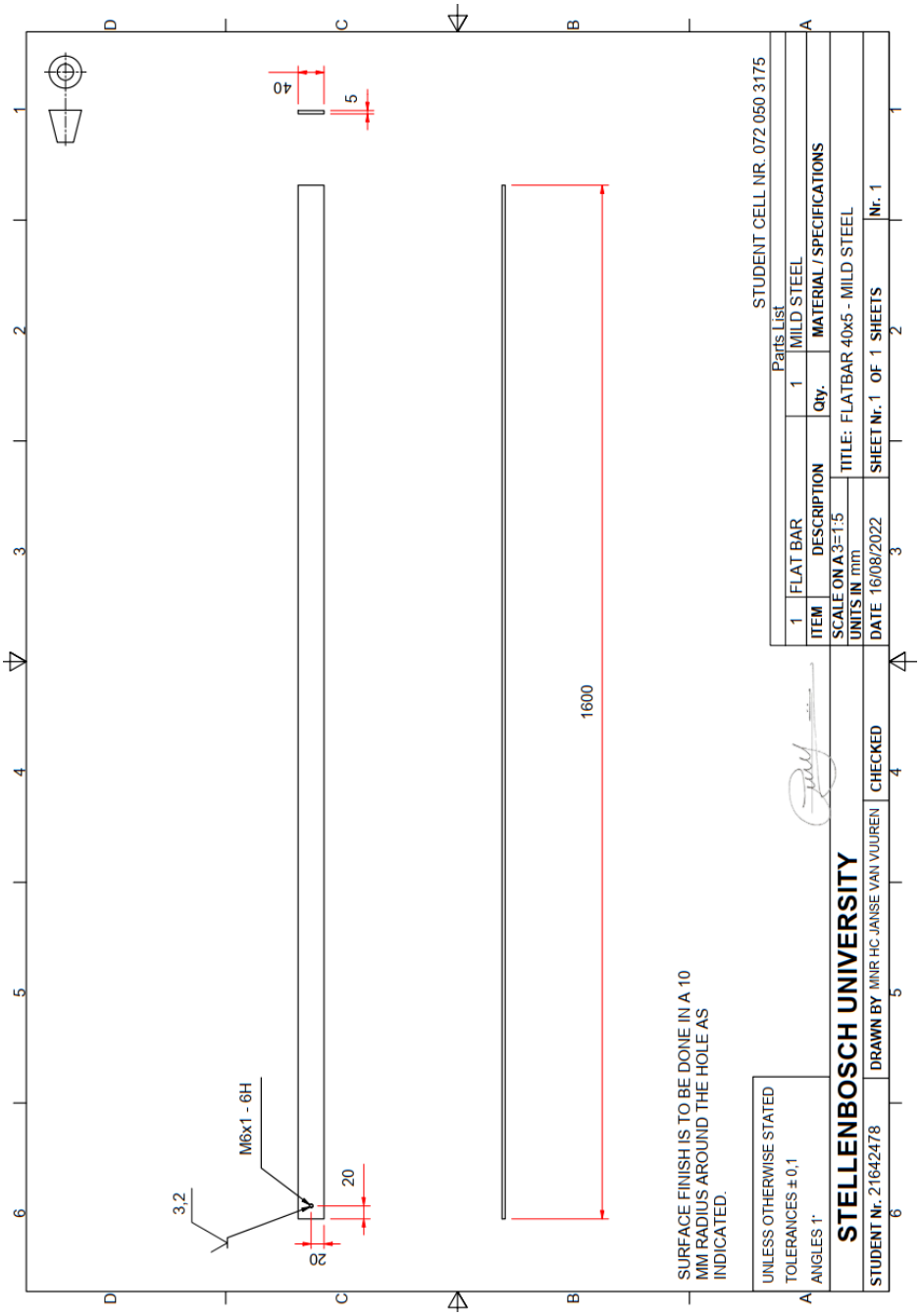

Figure 37: Test sample technical drawing

Appendix C Laboratory experiments safety report excerpts

Vibration Laboratory Safety Report

Modal analysis of I-beam

Date: 14/08/2022
Student: Mr HC Janse van Vuuren
Supervisor: Prof A Bekker
Lab Engineer: Mr J Laas
Head of Safety: Mr C Zietsman

Emergency Contacts:

Contact:	Room nr.	Work nr.	Cell nr.
Mr J. Laas	General laboratory	-	+27 83 462 9999
Mr C. Zietsman	M212	021 808 4275	-
Campus Security	-	021 808 2333	Whatsapp: 082 808 233
Fire Brigade	-	021 808 8888	-
Ambulance	-	021 883 3444	-

Signatures:

Student:
(HC Janse van Vuuren) _____

Supervisor:
(A Bekker) _____

Lab Engineer:
(J Laas) _____

Head of Safety:
(C Zietsman) _____

Pressure Vessels or Pipes: No pressure vessels or pipes with pressure in excess of 50kPa are involved in this project.

C.1 Safety report overview

The full safety report contains:

1. Overview of testing
    - 1.1 Aim of test
    - 1.2 Experiment setup
2. Detailed experimental procedure
    - 2.1 Steps for setup of experiment
    - 2.2 Experimental modal analysis steps
    - 2.3 Experimental fatigue life analysis steps
    - 2.4 Set down steps
3. General laboratory rules
    - 3.1 General laboratory safety
    - 3.2 General housekeeping
    - 3.3 Warning labels
    - 3.4 Fire safety
4. Risk assessment
    - 4.1 Activity based risk assessment
    - 4.2 Risk ratings

Appendix A Equipment list

Appendix B Emergency evacuation plan

Figure 1: Setup diagram for experimental modal analysis

Figure 2: Warning labels

C.2 Activity based risk assessment

Table 10: Activity based risk assessment

Activity	Risk	Risk Type (P/E)	Mitigating Steps
Moving test specimen	Dropping on hands	P	Keep hands clear of the bottom of the test specimen when moving, testing or suspending it.
	Dropping on feet	P	Wear steel toe shoes. Place a stable surface under the test specimen no more than 15 cm from its underside.
	Damaging wires	E	Make sure wires are out of the way before moving test specimen.
	Damaging sensors	E	Be aware of sensor locations and ensure that they will not be damaged when placing the test specimen before starting to move it.
Surface preparation	Scratching skin	P	Keep hand clear of area being sanded.
	Damaging skin with chemicals	P	Wear disposable gloves when working with chemicals such as the bonding catalyst.
	Improper surface preparation	E	Check resources and check with the laboratory engineer that the surfaces are in suitable condition before attaching sensors.
Sensor attachment	Improper attachment leading to inaccurate readings	E	Properly study literature and guides for proper sensor installation. Check with laboratory engineer before

			proceeding with testing.
Connecting sensors	Misidentifying a sensor	E	Label wires to ensure that the correct sensor is connected to the correct port on the DAS.
	Damaging wires	E	Secure wires with tape and only bend wires in gradual curves so they are not damaged.
Setting up and moving DAS and PC	Damaging equipment	E	Ensure equipment is placed on stable surfaces and that the path is clear when moving them. Ensure that nobody will move in areas where wires could be tripped on. Secure wires and power cords to the floor where movement is required.
Suspending the test specimen	Dropping the test specimen	P/E	Ensure that enough bungee cord is used for the weight of the test specimen.
Shaking the beam	Excessive shaker movement	E	Secure shaker to a stable surface.
Impacting the beam	Modal hammer overload	E	Set expected impact intensity through Testlab before testing.
Storing readings and data	Data loss	E	Backup data on an external hard drive.

C.3 Risk ratings

Table 11: Risk ratings

Activity	Risk	Likelihood	Exposure	Consequence	Score
Moving test specimen	Dropping on hands	4	6	3	72
	Dropping on feet	4	6	4	96
	Damaging wires	5	6	3	90
	Damaging sensors	4	6	5	120
Surface preparation	Scratching skin	5	3	1	15
	Damaging skin with chemicals	5	3	1	15
	Improper surface preparation	6	3	4	72

Sensor attachment	Improper attachment leading to inaccurate readings	6	3	4	72
Connecting sensors	Misidentifying a sensor	3	5	2	30
	Damaging wires	5	5	3	75
Setting up and moving DAS and PC	Damaging equipment	4	6	8	192
Suspending the test specimen	Dropping the test specimen	5	6	3	90
Shaking the beam	Excessive shaker movement	6	5	3	90
Impacting the beam	Modal hammer overload	6	5	3	90
Storing readings and data	Data loss	3	3	2	18

Appendix D Gantt Chart

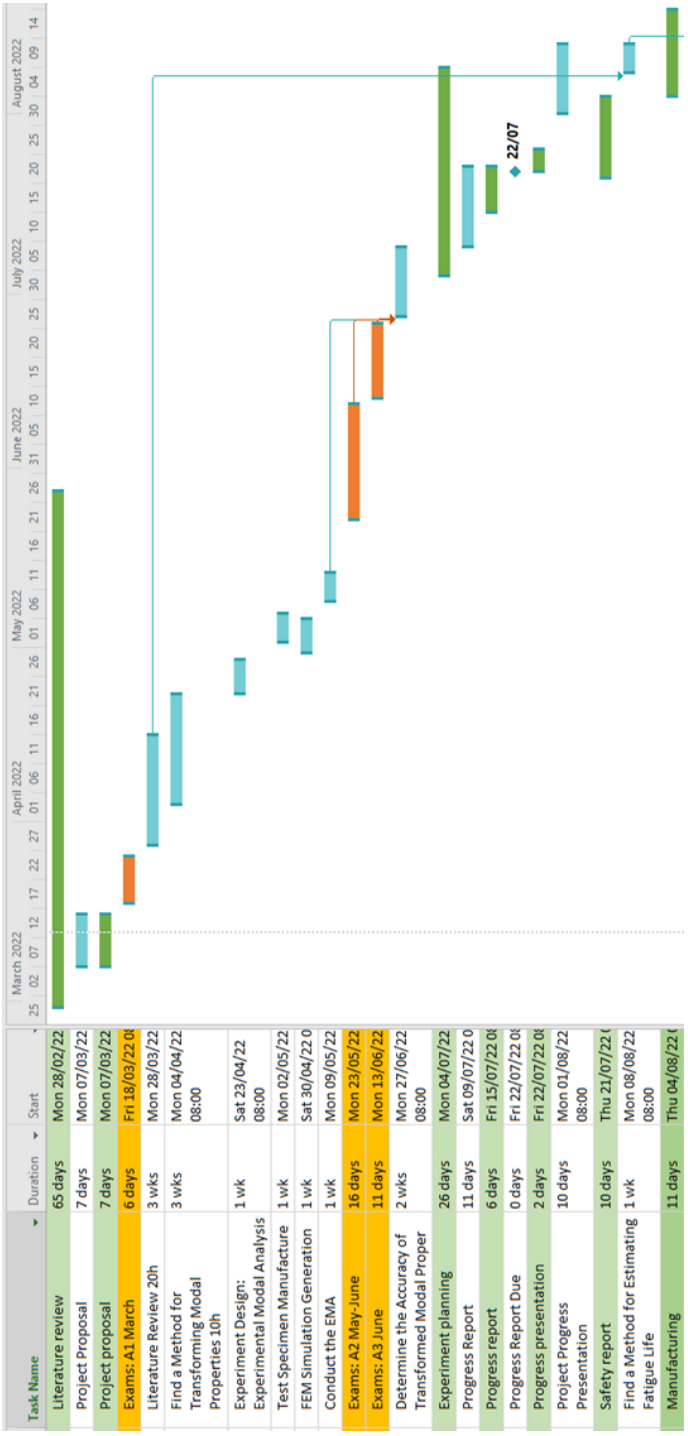

Figure 38: Project Gantt chart part 1- actual execution in green

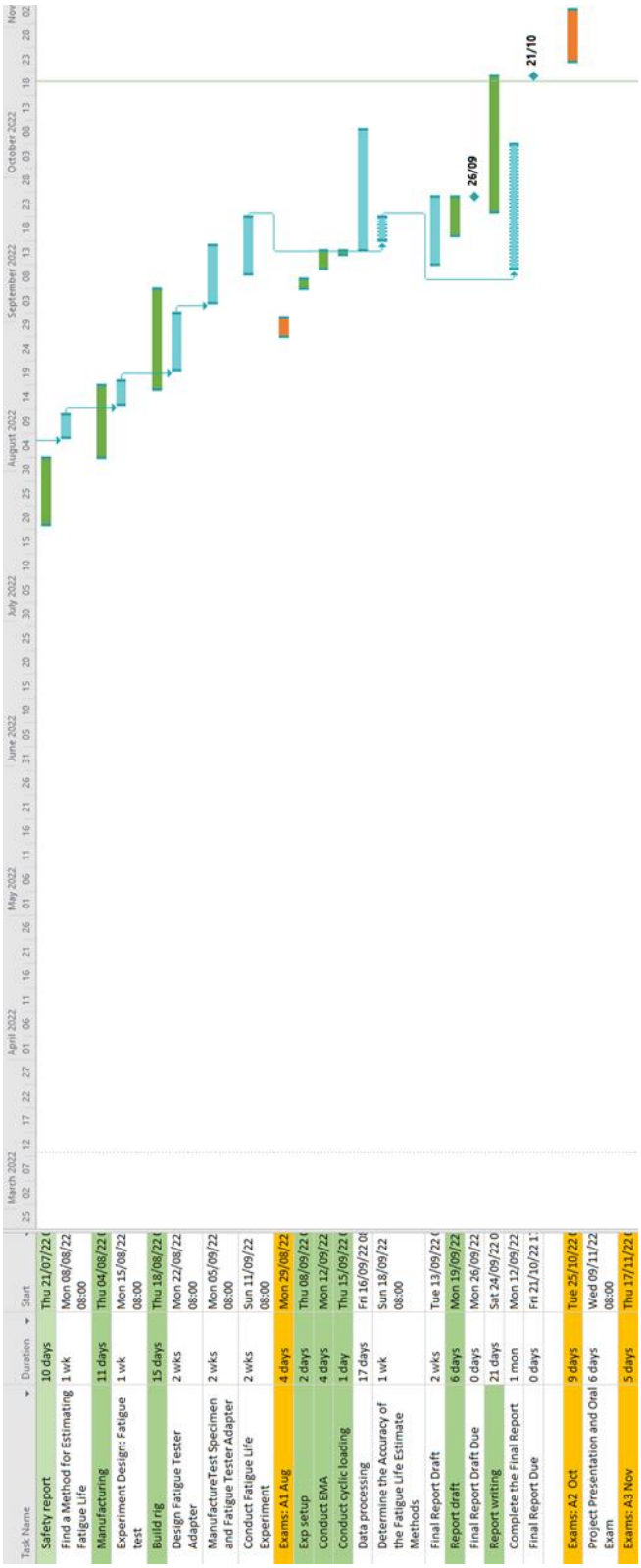

Figure 39: Project Gantt chart part 2 - actual execution in green

Appendix E Resource use and end-of-life strategy

Since our natural resources on Earth are finite, everyone has the responsibility to ensure that these resources are utilised responsibly and sustainably. This responsibility is especially big for engineers who design physical products.

In the case of this project, the only physical products designed was a test specimen for use in experiments and an experimental rig. This specimen is made of metal that can be sourced in South Africa. To ensure the responsible use of this material, the metal offcuts generated during the manufacturing process were collected for recycling. Before the end of the test specimen's life, it can be used in other projects for similar modal analysis and cyclic loading experiments. This ensures that new test specimens will not be manufactured unnecessarily. At the end of the test specimen's life, the used metal test specimens should also be sent for recycling to ensure that more use is obtained from the material.

This project was not very intensive in material resources, since the majority of the project consisted of the development and comparison of analysis methods and data processing.

Appendix F Techno-economic analysis

F.1 Expenses

Table 12: Planned expenses

Task Name:	Engineering Time		Running Cost	Facility Use	Capital Costs	MMW Labour		MMW Material	Total
	hr	R	R	R	R	hr	R	R	R
Literature Review	20.00	9 000.00	-	-	-	-	-	-	9 000.00
Find a Method for Transforming Modal Properties	10.00	4 500.00	-	-	-	-	-	-	4 500.00
Experiment Design: Experimental Modal Analysis	7.00	3 150.00	-	-	-	-	-	-	3 150.00
Test Specimen Manufacture	-	-	3 000.00	-	-	2.00	600.00	100.00	3 700.00
FEM Simulation Generation	5.00	2 250.00	-	250.00	-	-	-	-	2 500.00
Conduct the EMA	5.00	2 250.00	50.00	1 750.00	-	-	-	-	4 000.00
Determine the Accuracy of Transformed Modal Properties	10.00	4 500.00	-	-	-	-	-	-	4 500.00
Progress Report	15.00	6 750.00	-	-	-	-	-	-	6 750.00
Project Progress Presentation	5.00	2 250.00	-	-	-	-	-	-	2 250.00
Find a Method for Estimating Fatigue Life	10.00	4 500.00	-	-	-	-	-	-	4 500.00
Experiment Design: Fatigue test	10.00	4 500.00	-	-	-	-	-	-	4 500.00
Design Fatigue Tester Adapter	20.00	9 000.00	-	1 000.00	-	-	-	-	10 000.00
Manufacture Test Specimen and Fatigue Tester Adapter	-	-	300.00	-	-	5.00	1 500.00	500.00	2 300.00
Conduct Fatigue Life Experiment	10.00	4 500.00	100.00	2 500.00	-	-	-	-	7 100.00
Determine the Accuracy of the Fatigue Life Estimate Methods	5.00	2 250.00	-	-	-	-	-	-	2 250.00
Final Report Draft	30.00	13 500.00	-	-	-	-	-	-	13 500.00
Complete the Final Report	70.00	31 500.00	-	-	-	-	-	-	31 500.00
Project presentation and oral exam	10.00	4 500.00	-	-	-	-	-	-	4 500.00
Total	**242.00**	**108 900.00**	**3 450.00**	**5 500.00**	**-**	**7.00**	**2 100.00**	**600.00**	**120 500.00**

Table 13: Actual expenses

Task Name:	Engineering Time		Running Cost	Facility Use	Capital Costs	MMW Labour		MMW Material	Total
	hr	R	R	R	R	hr	R	R	R
Literature review	15.00	6 750.00	-	-	-	-	-	-	6 750.00
Project proposal	11.00	4 950.00	-	-	-	-	-	-	4 950.00
Experiment planning	92.00	41 400.00	-	-	-	-	-	-	41 400.00
Progress report	8.00	3 600.00	-	-	-	-	-	-	3 600.00
Progress presentation	7.00	3 150.00	-	-	-	-	-	-	3 150.00
Safety report	18.00	8 100.00	-	-	-	-	-	-	8 100.00
Manufacturing	3.00	1 350.00	50.00	-	-	1.00	300.00	52.00	1 752.00
Rig building	90.00	40 500.00	4 214.88	40.00	-	-	-	-	44 754.88
Experiment setup	9.00	4 050.00	-	-	-	-	-	-	4 050.00
EMA	18.00	8 100.00	100.00	9 800.00	-	-	-	-	18 000.00
Conduct cyclic loading	2.00	900.00	20.00	700.00	-	-	-	-	1 620.00
Report draft	12.00	5 400.00	-	-	-	-	-	-	5 400.00
Report writing	93.00	41 850.00	-	-	-	-	-	-	41 850.00
Project presentation and oral exam	10.00	4 500.00	-	-	-	-	-	-	4 500.00
Total	**388.00**	**174 600.00**	**4 384.88**	**10 540.00**	**-**	**1.00**	**300.00**	**52.00**	**189 876.88**

F.2 Discussion

The actual virtual budget ended up being far more than the planned virtual budget, in large part due to unrealistic time estimates during the project planning and proposal stage. Cost savings in engineering time and running costs were possible during the manufacturing of the experimental rig, by using less consumables such as solder tabs and strain gauges.

The increased virtual cost is in large part due to extra engineering time utilised during the project. Experimental rig construction took far more time than expected, and experiment planning could have been conducted in less time. The result was, however, a thoroughly instrumented test specimen and produced a fatigue analysis algorithm that can be utilised in future research.

This project informs the design of a future ship hull monitoring sensor network and generated knowledge for the sound and vibration research group of the Department of Mechanical and Mechatronic Engineering of the University of Stellenbosch. The successful design and implementation of a ship hull monitoring sensor network has great economic potential, since it can be used to inform remaining useful life estimates for operational marine vessels and be used as a performance metric for ship captains and marine logistic management.

At this stage, the algorithms and experimental rigs produced in this project cannot be commercialised as is, but can be used to inform the development of a commercial ship hull monitoring system.